Master's Thesis

Efficient domain integration of enriched elements using the moment fitting method enhanced by neural network

Taehun Kang

Department of Mechanical Engineering

Ulsan National Institute of Science and Technology

2022

Efficient domain integration of enriched elements using the moment fitting method enhanced by neural network

Taehun Kang

Department of Mechanical Engineering

Ulsan National Institute of Science and Technology

Efficient domain integration of enriched elements using the moment fitting method enhanced by neural network

A thesis/dissertation submitted to
Ulsan National Institute of Science and Technology
in partial fulfillment of the
requirements for the degree of
Master of Science

Taehun Kang

12.14.2021 of submission

Approved by

Advisor
Hayoung Chung

Efficient domain integration of enriched elements using the moment fitting method enhanced by neural network

Taehun Kang

This certifies that the thesis/dissertation of Taehun Kang is approved.

12.14.2021

Advisor: Hayoung Chung

Wooseok Ji

Im Doo Jung

Abstract

To avoid re-meshing in the analysis of multiphase structure including dissimilar materials or fluid interfaces, the non-conforming mesh is typically used. Since the elements involve discontinuities, various enrichment strategy was presented to approximate the solutions such as kinks, jumps, singularities, and other non-smooth features. Yet, the enriched element requires a heavy computational load due to the increment of the quadrature points. Herein, we introduce a novel method that further accelerates the adaptive quadrature method by employing the artificial neural network. The adaptive quadrature, namely the moment fitting method and selective enrichment strategy has been proposed to reduce the computational load by fixing the number of quadrature points in the enriched element. Computing the weighting factors of the moment fitting method is a burdensome process, however, the computational overhead is thereby minimized since the calculation of the moments is now substituted by a neural network. The discontinuity within the enriched elements is implicitly represented by the nodal level set values, which are discretized by the FEA grid. Required moments are then regressed adaptively by the neural network based on the level sets without heavy computation. Moreover, we improve the solution accuracy without increasing the FEA grid by detaching the level set grid from the FEA grid. The level set grid of the enriched element constructed higher resolution of FEA grid, enables a detailed representation of the enrichment. After detaching the level set grid, more accurately the weighting factors of the moment fitting method can be obtained since the integration of the enriched element is executed by a constant number of quadrature points. The accuracy and efficiency of the proposed method are demonstrated by solving several numerical examples. Further, the proposed method can be applied in the perspective of the topology optimization, the homogenization method, or three-dimensional extension in terms of high computing efficiency.

Contents

List of Figure

List of Table

Chapter 1. Introduction

1.1 Research background

In structural mechanics, discontinuity is issued in the inhomogeneity of the structures (e.g., singularity). Broadly, there are two categories; weak and strong discontinuities. Weak discontinuity roughly indicates the discontinuity of stress and strain fields. For instance, interfaces located in dissimilar material properties in solid mechanics or interfaces in two-phase flow in fluid mechanics. On the other hand, strong discontinuity refers to the jumps in the displacement field, like cracks or voids. The solution fields of these discontinuous problems are singular across the discontinuity.

In numerical modeling of such discontinuity problems, FEA for example, the mesh configuration is generated along the boundary to enable the interpretation of the discontinuous phases. Which suggests aligning the inter-element boundary and the boundary of discontinuous fields assuming the homogeneity of the materials inside the mesh. In this regard, the body-fitted mesh is typically used in finite element analysis. However, the conforming mesh is often burdensome while handling complex geometries or requiring remeshing due to the change of interfaces during analysis. For instance, in the case of the crack front (strong discontinuity) or changing the interfaces between dissimilar materials (weak discontinuity), the boundary of the singularity continuously evolves or changes, which causes exacerbation of the computational overhead.

To cover the issues mentioned above, various techniques using a non-conforming mesh that retains the configuration of the mesh, regardless of the geometric characteristics of the domain have been proposed widely. Meanwhile, the discontinuity appears inevitably within the elements in the non-conforming mesh, arises the solution space involves discontinuity, singularities, and other non-smooth features. In order to cope with such non-smooth features, various approaches have been proposed including ersatz material modeling, the extended finite element method, the general finite element methods, and finite cell methods. Except for the ersatz material method, these methods embed additional functions to represent the discontinuity or singularity within the element known as the enrichment function. The enrichment technique includes the extra degree of freedom to the solution field for the asymptotically reproducing the singularity of discontinuity, (e.g., crack propagation and topology optimization) due to the capability of using different enrichment functions tailored upon the type of discontinuity.

Babuska et al. [1, 2] first introduced a partition of unity method in finite element analysis. Belytschko et al. [3] presented the extended finite element method, as one of the partition of unity methods that extends a classical approximate solution based on a set of enrichment functions that implies the features of the solution fields (e.g., singularity, discontinuity). In a similar perspective, Strouboulis [4,5]

introduced a generalized finite element method, related to the partition of unity concept. Moës et al. developed modeling crack growth with enrichment strategy in [8]. Also, the author first combined the extended finite element method and the level set function as signed distance function in [6,7], and proposed a new framework of the enrichment strategy to capture the geometry of discontinuity in the interfaces at [9]. Sukumar et al. [10] presented the methodology of modeling arbitrary holes and material interfaces without meshing the internal boundaries by combining the level set method and the extended finite element method. The enrichment function can be determined depending on the asymptotic solution space while not negating solution convergence. For instance, the displacement solution space of strong and weak discontinuity (e.g., crack propagation, material discontinuity) could be represented as, but only the enriched function is expressed differently for each solution. The author also presented 3D crack modeling in [11], demonstrating the accuracy of the extended finite element method. Aragón [12] recently introduced a Discontinuity-Enriched Finite Element Method (DE-FEM), which adds the enriched degrees of freedom assign to new nodes created along the discontinuity within the elements instead of the original mesh. Lang et al. [13] proposed the preconditioning scheme to avoid the ill-conditioning system of the enriched elements. Similar work was presented by Bechet et al., which also suggested the preconditioning of the ill-posed elements that have relatively small geometric area compared to the domain area [14]. Sauerland et al. [15] introduced a stable XFEM to handle the circumstance of ill-conditioning often occurring in XFEM, originally proposed by Babuska [16]. The author proposed another enrichment function in s-XFEM that linear interpolant of the global enrichment function, leading to reducing the condition number of the enriched element as standard FEM. The author also proposed the standard of the ill-posed condition of the enriched element (i.e., area or volume ratio of the subdivisions occupied in the enriched element).

In the viewpoint of numerical modeling, however, the enrichment techniques require expansive computational costs. The integration of the discontinuous domains of the element is essential to obtain the stiffness within the non-conforming mesh. The integration accuracy, however, is inevitably reduced. It is not easy to integrate non-standard functions, but it also significantly impacts computational efficiency, not solution accuracy. The enrichment strategy requires expensive computational costs when the number of enriched elements increases. The approximate solution space in the enriched element does not allow the use of the standard Gauss quadrature method used in standard finite element methods because the integrand function is no longer polynomial form. Accordingly, the number of Gauss quadrature points increases substantially in the enriched domain. In XFEM, which uses nodal enrichment of the rigid-centered function to account for material interfaces, utilizes a subdivision technique in which enriched elements are subdivided into several simplicial elements to secure the homogeneity within the sub-elements. Fries [17,18] introduced the integration method of such sub-

divided elements into triangles and used piecewise linear interfaces. Thus, the sub-elements are always polygonal, easily obtaining the integrations of enriched elements. By doing so, it is beneficial in the sense that the standard Gauss quadrature method is applied and simplifies the method. However, the computational overhead inevitably increases as the number of Gauss quadrature points increases if the increment of these sub-elements.

Meanwhile, a quadrature rule for integrating arbitrary domain was developed by Mousavi [19] namely the moment fitting method. Originally, the moment fitting equation which contains the integrations of the basis functions has been used to find the regions of the triangles [20, 21]. Mousavi et al. [19] first present the numerical integration by means of the moment fitting method in finite element analysis, and also in [22], introduced a method that solves the moment fitting equation and obtains the corresponding weights where desired quadrature points. Muller [23] presented a variant of the moment fitting method, in which quadrature rules were derived in the element cut by the geometric representation in terms of the level set functions. Hubrich introduced the finite cell method based on the moment fitting method [24], and this work was extended to the arbitrary shape and topology in 3D by the [25]. Also, the author introduced the integration scheme based on the moment fitting method and smart octree to reduce the quadrature points [26]. Furthermore, the author presented a new moment fitting approach [27] by choosing the quadrature points as Lagrange polynomial through Gauss-Legendre points to solve the moment fitting equation as a linear system and applied it in nonlinear problem. Thiagarajan et al. [28] presented an adaptively weighted numerical integration scheme that utilizes the moment fitting method to increase the computational efficiency of the classical cell method. Zhang et al. [29] presented a new quadrature scheme based on the moment fitting method for integrating the discontinuities on an arbitrary domain in 3D, also presented the method of retaining strictly positive weights by the volume fraction approach. Bui et.al. [30] applies the moment fitting weights in nonlinear iteration using the fact that it can be re-usable, while obtaining the moments in a way of well-known quadrature based on the adaptive subdivision. Lately, Düster et al. [31] proposed a method, the selective enrichment and utilizing the moment fitting method either, demonstrating 1D bar problem, remaining further extensibility of 2D or 3D. The main idea of the paper, the selective enrichment approach, requires the integration of various types of functions, which are components of the stiffness matrix. Also, adapting the moment fitting method to fix the number of integration points within the elements containing the discontinuity. This method shows sufficient accuracy with the minimal number of integration points if the calculation of moments becomes exact. However, establishing the quadrature of the moment fitting system is a necessary but burdensome process, which aggravates the computing efficiency.

Besides, under the assumption of the exact calculation of the right-hand side of the moment fitting

system already mentioned is obtained, we figure out the moment fitting method can produce the same or even more accurate results as comparing the existing XFEM-like integration method while reducing the number of quadrature points. In this respect, we investigate the grid separation technique for precise representation of discontinuity of the structure. The level set grid and finite element grid are considered separately, where the level set grid is utilized only to express the rigorous of discontinuity. Because of detaching of the grids, extra nodal level set information of discontinuity within the element can be considered, resulting in a more accurate depiction of discontinuity. The computation of the moment fitting weights can be obtained by an accurate integral of the right-hand side of the moment fitting system, and it allowed us to get better results compared to before. In addition, some of the ambiguous problems that could not be solved by the existing XFEM with limited level set information have been solved.

Recently, AI-related methods rapidly improved as well as the development of computing power. Many works introduce the accurate surrogate of a high fidelity network model at an unprecedented efficiency. The remarkable success of the deep learning technique in various engineering disciplines is due to its performance in handling a large dataset to realize assimilation of these data. A number of artificial neural networks have been presented to accelerate the numerical analysis or very versatile regression method and also used in the offline computation. Im et al. [32] utilize the feedforward network to the constitutive model of crystal structure based on the strain data of hyperelastic crystal structure. The regression model of the paper can even estimate better performance in some manner. Wei [33] presents a physics guided neural network framework where the regression model is based on the purely data-driven displacement, potential energy based and governing PDE based in FEM. Xiao et al. [34] used a feedforward network for the estimation of the current density based on the electric field vectors of the graphene volume fraction within the typical volume of microstructure. The highly nonlinear relationship of those is efficiently evaluated by the surrogate neural network model, to reduce the computational time dramatically. Kim [35] introduced a specific numerical method to speed up the overall analysis where using the network estimates the iterative convergence of the Newton-Raphson method in the nonlinear problem. Such studies demonstrated the high efficiency and efficacy of the neural network model of replacing whole or part of the computation. It is worth noting that while varying in purpose, most of these regression models requires intrusive changes to the existing methods. The usability of these techniques, despite their great potentials, thus requires a drastic shift of the existing analysis or design process hence are limited in the actual usage. Further, the context of analyzing structure with discontinuity-related works does not present yet.

1.2 Research objective

This work aims to resolve a computational bottleneck found in the domain integration of discontinuous elements by replacing an expensive routine with the surrogate model created by the neural network. An expensive calculation of the required moments (i.e., the bottleneck in analysis) of the selective enrichment approach is executed in advance to reduce the computational overhead of the analysis further. The vast amount of data accumulated, however, is not directly used or interpolated but regressed by the network. It is possible because the implicit domain representation is done by the level set function. To cover the entire range of the level sets, data preparation is performed and the required moments are regressed depending on the nodal level set values. Training of the network is based on the pre-calculation of the enriched element, especially the feature of the enrichment is implied in the network for substituting the numerical computation. The pre-trained neural network can regress the computed moments in the moment fitting method to online finite element analysis. After constructing and training the network, we regressed the moments in the analysis (i.e., on-the-fly computation), replacing the calculation of moments to the trained neural network, the bottleneck of the moment fitting method can be resolved. Moreover, thanks to the fixed number of quadrature points, detachment of the level set and FE grid can be applied. The resolution of the domain representation is thereby increased. The detached level set grid is only utilized for the representing of precise discontinuity. The accuracy of the representation is therefore not limited by the resolution of the finite element grid, which is strongly tied with a computation capacity. The solution accuracy is even enhanced to the degree where the level set-related ambiguity emerges, with a marginal addition of computational load. A few tests of the enriched cases are demonstrated for checking the network, and the model is applied in several numerical examples. Considering the further expansion of this work, we design the network to be utilized not limited to a particular problem but in other aspects (e.g., topology optimization, homogenization).

1.3 Thesis organization

In Chapter 2, we first investigate a typical method for representing the discontinuity in the domain of interest as the level set method. Then the well-known technique, XFEM, is introduced as the fundamental concept of the enrichment strategy. The overall concept of selective enrichment in [31] and the implementation of the moment fitting method are described either. Also, the artificial neural network which is for the regression of the proper moments in the online stage of the finite element analysis is introduced. Lastly, in Chapter 3, four numerical examples are demonstrated regarding the accuracy and efficiency of the network model. Further extensibility and applicability are also manifest through other examples.

Chapter 2. Methods

In this chapter, we introduce the outline of the finite element method used in this study. The representation of discontinuity of the materials using the level set method is first addressed. Next, the enrichment strategy using non-conforming mesh and finite element formulation is introduced. This is directly related to the selective enrichment and the integrand of the moment fitting method. Lastly, computation of the moment fitting weights and regression with the artificial neural network is presented.

2.1 Representation of discontinuity

Considering the elastic structure that consisted of bi-material such as inclusions, for instance, the domain of interest Ω is then regarded as $\Omega = \Omega_1 \cup \Omega_2$ as illustrated in Figure 2.1.1. The interface of two dissimilar materials Γ is defined between domain Ω_1 and Ω_2. The implicit representation of each domain can be stated as a level set function $\phi(X)$, where X is defined as an arbitrary point within the domain Ω. The interface Γ and each domain is represent as

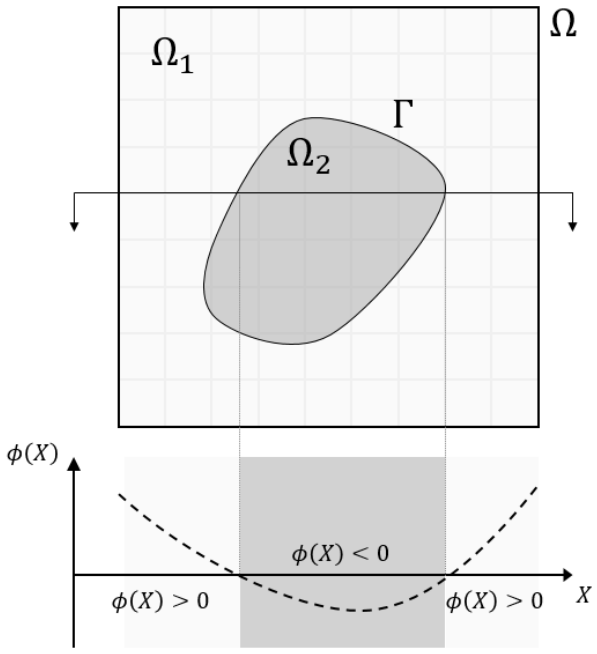

Figure 2.1.1 Domain representation by level set function $\phi(X)$.

$$\begin{aligned} \phi(X) > 0 \;\; if \;\; X \in \Omega_1 \\ \phi(X) < 0 \;\; if \;\; X \in \Omega_2 \\ \phi(X) = 0 \;\; if \;\; X \in \Gamma \end{aligned} \tag{1}$$

Notably, depending on the sign of $\phi(X)$, the representing domains can be reversed, and the zero-value of $\phi(X)$ implicitly denotes the interface Γ within Ω. The level set grid implicitly demonstrates the boundary of the structure, however, it is worth mentioning that after discretization of finite element mesh, the level set grid and finite element grid are not necessarily equivalent in this work. Meaning the solution space of the structure is formed based on the finite element grid, and the level set grid is used only to represent the interface. As will be discussed later, the finite element grid and the level set grid are considered separately as a way to increase the solution accuracy and the resolution of the interface without increasing the computational overhead.

2.2 Enriched element formulation

For the purpose of the present work, the non-conforming mesh is used in finite element analysis. Moreover, we treat quadrilateral element type which is broadly used. A displacement field U of the solution space is assumed as continuous in Ω, but it does not while in Γ. Herein, apart from the classical finite element method, the displacement field $U^{enriched}$ is defined as obtaining the additional enriched degree of freedom a as mentioned in Chapter 1.

$$U^{enriched} = Nu + NFa \tag{2}$$

Where N is the shape function of isoparametric elements, u is standard FE displacement DOF, F is the enrichment function that incorporates the special case about the solution (e.g., kink, jumps, singularities). And a is an enriched degree of freedom, which is non-zero only for the element containing material interfaces (i.e., enriched element). In this work, we use the enrichment function F considering a weakly discontinuous interface, and containing the kink of the solution space. Although the proposed scheme is not limited to this specific case, the overall method is straightforwardly extended to the other type of discontinuity, once another types of enrichment function is employed (e.g., heaviside function for the strong discontinuity). The enrichment function F throughout this work is defined as

$$F(X) = \sum_i N_i|\phi_i| - \sum_i |N_i\phi_i| \tag{3}$$

Where ϕ_i indicates the level set value found at node i. The choice of the enrichment function $F(X)$ is already suggested in [9]. The enrichment function $F(X)$ has a ridge centered shape at the interface and zero value at non-enriched elements. The configuration of the $F(X)$ in 1D and 2D is illustrated in Figure 2.2.1

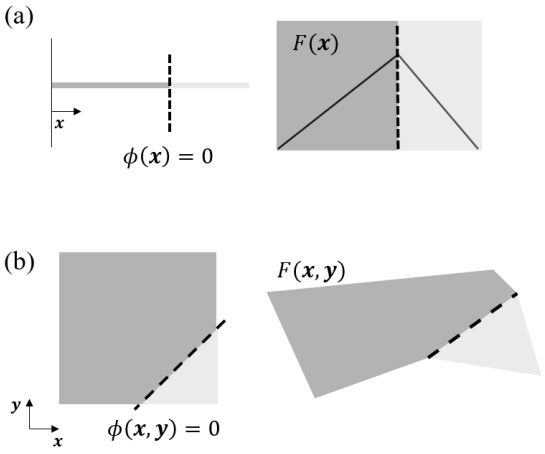

Figure 2.2.1 Configuration of the enrichment function $F(X)$ in (a) 1D, (b) 2D.

Although the simplest kink enrichment function is utilized in this work the proposed method is not limited to such weak discontinuity but is able to extend other cases of discontinuity problems by changing the $F(X)$; Heaviside function, for instance, in crack propagation. Employing the standard Galerkin method in (2), the stiffness matrix $\boldsymbol{K}$ and the force vector $\boldsymbol{f}$ becomes

$$\boldsymbol{K} = \begin{bmatrix} K_{uu} & K_{ue} \\ K_{eu} & K_{ee} \end{bmatrix}, \boldsymbol{f} = \begin{bmatrix} f_u \\ f_e \end{bmatrix} \tag{4}$$

Where subscript u and e denotes the components that related to either DOFs of pure displacement u and enrichment a respectively. The detailed form of $\boldsymbol{K}$ is

$$\boldsymbol{K} = \int_{\Omega_e} \boldsymbol{B}^{\boldsymbol{T}} \boldsymbol{C} \boldsymbol{B} d\Omega_e \tag{5}$$

Where $\boldsymbol{B}$ is strain displacement matrix, and $\boldsymbol{C}$ is constitutive matrix respectively. For simplicity, we assume the same Poisson`s ratio of dissimilar materials within the enriched element, which leading $\boldsymbol{C}$ is now the function of single variable, $E(r)$, the Young`s modulus, where r indicate the reference coordinate of the enriched element. Accordingly, the local stiffness matrix $\boldsymbol{K}$ and load vector $\boldsymbol{f}$ has a form of

$$K_{uu} = \int_{\Omega_e} (\nabla N)^T E(r) (\nabla N) d\Omega_e \tag{6}$$

$$K_{ue} = \int_{\Omega_e} (\nabla N)^T E(r) (\nabla NF + \nabla FN)\, d\Omega_e \tag{7}$$

$$K_{ee} = \int_{\Omega_e} (\nabla NF + \nabla FN)^T E(r) (\nabla NF + \nabla FN)\, d\Omega_e \tag{8}$$

$$f_{uu} = t \int_{\Omega_e} N d\Omega_e \tag{9}$$

$$f_{ue} = t \int_{\Omega_e} NF d\Omega_e \tag{10}$$

Where t is traction vector. The components of the stiffness matrix $\boldsymbol{K}$ and force vector $\boldsymbol{f}$ constructs in several types of integrands. The exact integral of each term provides the desired solution accuracy while making more accurate $\boldsymbol{K}$ and $\boldsymbol{f}$. However, the typical quadrature is no more applicable, because the integrand of each term in $\boldsymbol{K}$ is not a typical polynomial. So in the XFEM method [17], the domain of the enriched element Ω_e is split into several sub-regions to the homogeneity of the sub-region is obeyed, then the standard Gauss quadrature rule applies. This approach often requires high computational cost while the number of integration points increases, and further burdensome when the problem requires iterative computation.

2.2.1 Selective enrichment and the moment fitting method

In this work, we use the adaptive weight calculation technique presented by Duster [31], namely the

moment fitting method with selective enrichment, to integrate the enriched element. The moment fitting method is a quadrature rule for arbitrary function integration. The matrix form of moment fitting equation is

$$\begin{bmatrix} f_1(r_1) & \cdots & f_1(r_n) \\ \vdots & \ddots & \vdots \\ f_m(r_1) & \cdots & f_m(r_n) \end{bmatrix} \begin{bmatrix} w_1 \\ \vdots \\ w_n \end{bmatrix} = \begin{bmatrix} \int_{\Omega_e} f_1(r) d\Omega_e \\ \vdots \\ \int_{\Omega_e} f_m(r) d\Omega_e \end{bmatrix} \tag{11}$$

Where r_i $(i = 1,2, \dots, n)$ and w_i are the location and a quadrature weight of index i respectively. Ω_e denotes the integration domain, that is, the domain of the enriched element. A set of integrand f_j $(j = 1, \dots, n)$ denotes n basis function. Note that the method is reduced to a well-known Gauss-Legendre quadrature when the integrand function f is Lagrange polynomial through Gauss-Legendre points. A careful selection of the integrand function f is essential for the construct accurate quadrature of (11). Therefore, different integrand function f_j are defined according to Duster [31].

$$f_j = H_j(r)P(r) \tag{12}$$

Where $P(r)$ is Lagrange polynomials through pre-defined quadrature points. In 2D case, $P(r)$ can be written as

$$P(r) = \prod_{k=1, k \neq l}^{n} \frac{x - x_k}{x_l - x_k} \cdot \prod_{p=1, p \neq q}^{n} \frac{y - y_p}{y_q - y_p} \tag{13}$$

Throughout this work, we use a Lagrange polynomial of order 2 in both x and y directions (i.e., n=3). Function $H_j(r)$ defined as the different types of integrand in (4).

$$H_1(r) = E(r), \quad H_2(r) = F(r), \quad H_3(r) = E(r)F(r), \quad H_4(r) = E(r)F(r)^2$$
$$[H_5(r); H_6(r)] = E(r)\left[F_{,x}(r); F_{,y}(r)\right], \quad [H_7(r); H_8(r)] = E(r)F(r)\left[F_{,x}(r); F_{,y}(r)\right] \quad (14)$$
$$[H_9(r); H_{10}(r)] = E(r)\left[F_{,x}^2(r); F_{,y}^2(r)\right], \quad H_{11}(r) = E(r)F_{,x}(r)F_{,y}(r)$$

The types of function $H_j(r)$ are the integrand terms that appear in the stiffness matrix and force vector of the enriched element. The selected integrand function f in the moment fitting method has a polynomial multiplied by a discontinuous function $E(r)$ and $F(r)$ or $F_{,X}(r)$ (i.e., $H_j P^i$). Detailed configuration of selected integrand function of the enrichment in Figure 2.2.1 (b) is shown in below.

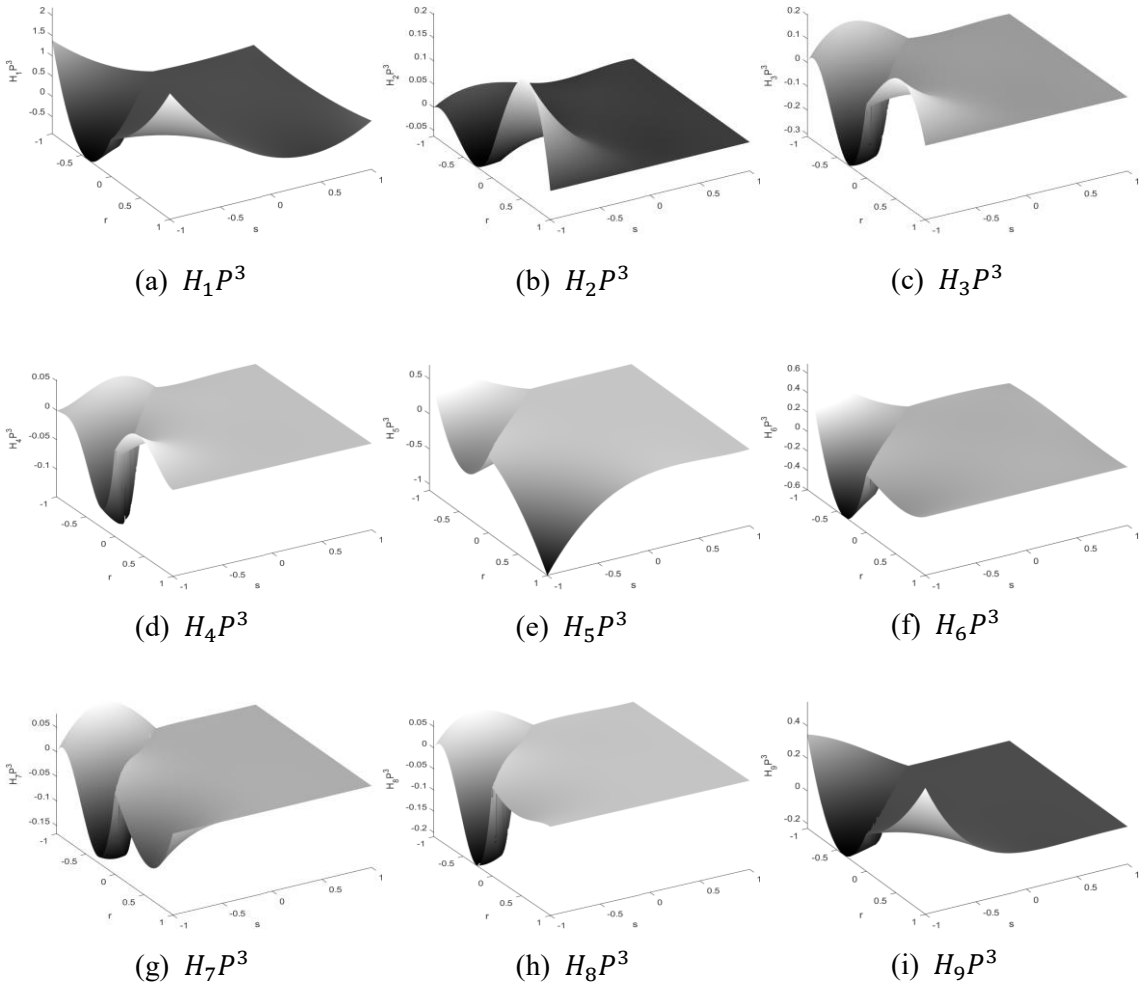

(a) H_1P^3 (b) H_2P^3 (c) H_3P^3

(d) H_4P^3 (e) H_5P^3 (f) H_6P^3

(g) H_7P^3 (h) H_8P^3 (i) H_9P^3

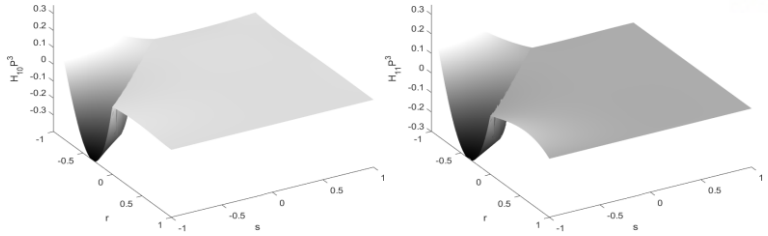

(j) $H_{10}P^3$ (k) $H_{11}P^3$

Figure 2.2.2 Different types of integrand H_jP^i, where $i = 3$ and (a) $j = 1$, (b) $j = 2$, … (k) $j = 11$ respectively.

Selecting the integrand function f as H_jP^i, the coefficient matrix of (11) becomes diagonal, because of the orthogonality of the Lagrange polynomials and pre-defined Gauss Legendre quadrature points. Therefore, the computation of the moment fitting equation reduces as

$$w_j^i = \frac{\int_{\Omega_e} H_j(r)P^i(r)d\Omega_e}{H_j(r_i)} \tag{15}$$

The abscissas and corresponding weights calculated based on the (15) illustrated in Figure 2.2.3.

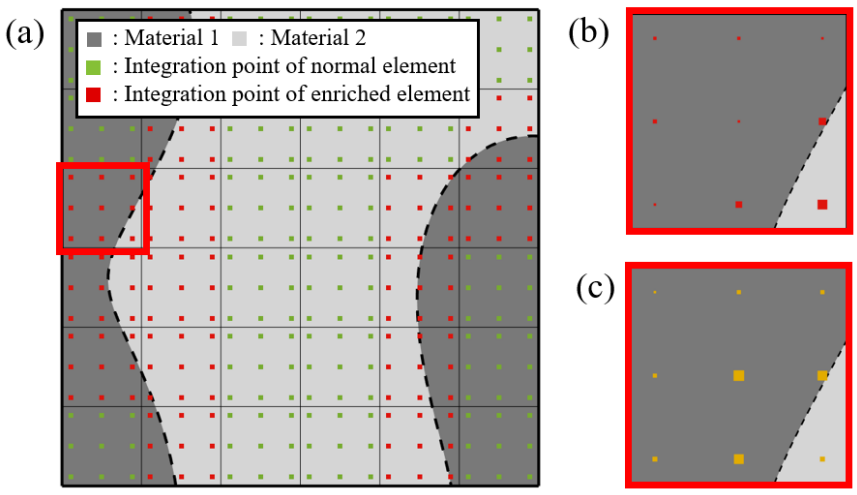

Figure 2.2.3 Quadrature point of the structure is shown in (a) and weighting factors of integrand type I_1 and I_2 are illustrated in (b) and (c) respectively.

The black and gray colors and their interface is represented in broken lines. As shown in Figure 2.2.3, the number of integration points found in those of the enriched element (red dot) and otherwise (green dot) remain constant. The green dots represent the standard Gauss quadrature weights, while the red dots represent the moment fitting weights. The magnitudes and location of moment fitting weights, (i.e., $w_1^1, \dots, w_1^9$ and $w_2^1, \dots, w_2^9$) of the enriched element (red box) is visualized in Figure 2.2.3 (b) and (c). The moment fitting weights of the enriched element is strongly dependent on the types of the integrand $H_j(r)$, and the shape of enrichment. Herein, the exact integration of I_i is the key point to get moment fitting weight, since the type of function H_j is nontrivial and various shapes of enrichment to be considered. Ideally, handling of the symbolic domain integration can provide the highest accuracy. However, in our experience, this approach is inappropriate because of computational efficiency. In the numerical experiment, the symbolic calculation of a two-dimension enriched element requires more than 10 seconds to evaluate moment fitting weights, equipping Intel i7-9700K and DDR4 32GB RAM. Accordingly, the integration of such requires a more efficient method: although there are plenty of other approaches to evaluating the integration. (i.e., Simpson`s method, sub-cell method). In this work, we employ the sub-partitioning method used in XFEM method. The integrand which form of $H_j P^i$ was numerically evaluated while maintaining homogeneity of sub-partition of the domain. To investigate the differences between the methods of XFEM and MF, the relative error between them is measured.

$$e_r = \frac{|I^{XFEM} - I^{MF}|}{I^{XFEM}} \tag{16}$$

Where I^{XFEM} and I^{MF} denotes the domain integration of each integrand type (i.e., $j = 1, \dots, 11$) of XFEM and the moment fitting method respectively.

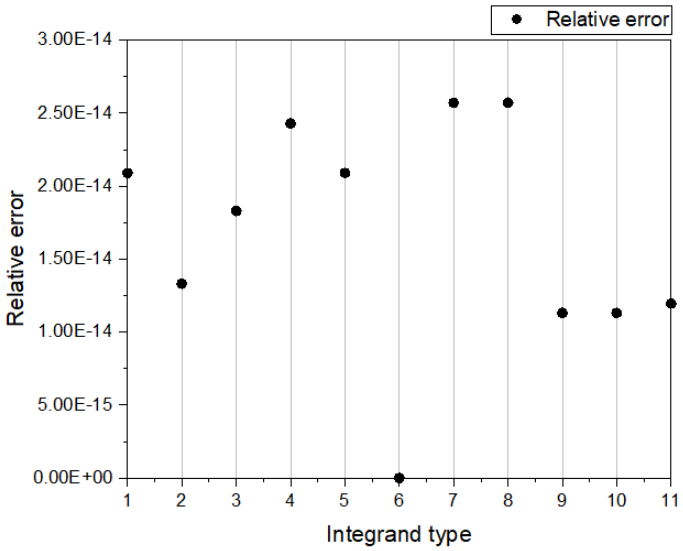

Figure 2.2.4 Relative error of XFEM and the moment fitting method respect to the integrand type I_1 to I_{11} of the enriched element shown in Figure 2.2.1 (b).

As shown in Figure 2.2.4., the relative error of the integrand computed by the XFEM and MF method is below 3×10^{-14}. This means the stiffness matrix and force vector terms computed by the moment fitting method are equivalent enough to those of the XFEM method. The main question is the approach of obtaining the weighting factors of the moment fitting method. The exact calculation of the weights (15) guarantees the desired accuracy of the integration.

In the present section, methods used to reduce the computational cost induced by the moment fitting method, while preserving the overall solution accuracy, are introduced. We first address a way to increase the solution accuracy only by modifying the domain where $\int_{\Omega_e} f(r) d\Omega_e$ is integrated. Having no need to change the analysis routine, including the number of Gauss quadrature points and elements, the accuracy increase is achieved without extra cost. Secondly, we present a way to circumvent the moment fitting procedures by calculating weights in the analysis procedure (i.e., offline stage). The complex relationship between the level set values and the moment fitting weights is trained within the artificial neural network, which appears as the nonlinear regression.

2.2.2 Adaptive resolution in structural representation

To increase the accuracy of the integrations of the moment fitting system (11), we only increase the resolution of the level set grid by *h-adaptivity*, leaving one of the finite element grid unchanged discussed in Chapter 1. Specifically, only a function of $E(r)$ is modified to accommodate such change. The integration domain, on the other hand, is firstly divided based on the level set grids found in the corresponding finite element. Each of the level set based sub element is then integrated based on the sub-partitioning scheme discussed in Chapter 2.2. The weights (i.e.,w_j^i), are obtained based on (15), where all the variables are evaluated on the finite element grid, and used without any further change.

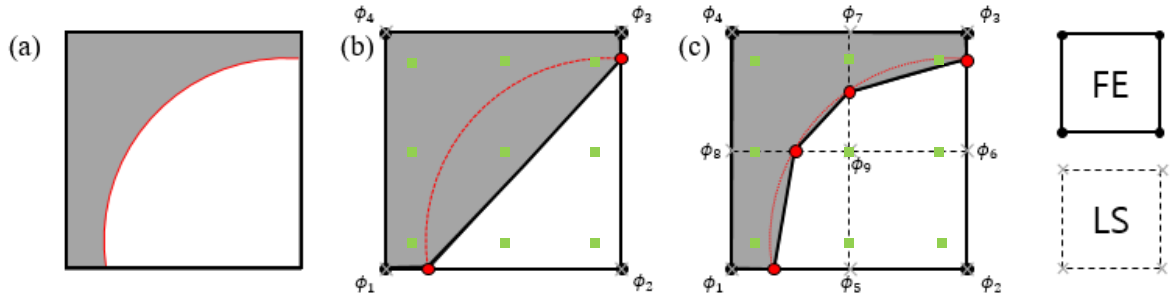

Figure 2.2.5 Effect of using different grid of level set (dotted lines and cross markers) and finite element (solid lines and circle markers) grids: (a) Enriched element; (b) Quadrilateral enriched element with 4 level set values; (c) Quadrilateral enriched element with 9 level set values.

Figure 2.2.5 depicts the modified integration procedures and the increased accuracy in domain integration by using different level set (dotted line) and finite element (solid line) grids: If the material interface has a high curvature as shown in Figure 2.2.5 (a), the sub-partitioning scheme and XFEM method likewise fail to reflect such interface because of the assumed straight interface (Figure 2.2.5 (b)), which bring the inaccuracy of I_i. The level set function is therefore separated from the finite element grid and the resolution is increased as shown in Figure 2.2.5 (c), hence the integrated values of I_i better reflect the curvy interface. The finite element nodes (solid dots) and their connectivity retain as these in Figure 2.2.5 (b), and so as the number of quadrature points; therefore, the computational load needed to solve the state equation remains constant. It is worth noting that there are no shared level set elements found within different finite elements, (e.g., ϕ_1 to ϕ_4 should lie on each node), and the resolution of the level set representation should have equal or higher than that of the finite element grid.

Abscissas r	Abscissas s	Symbolic	4 nodal level set	9 nodal level set
-0.774596	-0.774596	2.4214388	1.8343199	2.2514571
-0.774596	0	5.0215168	5.0380094	5.073770
-0.774596	0.774596	3.1071836	3.0940559	3.0599347
0	-0.774596	0.1585558	0.00014381	0.1377572
0	0	3.1496040	2.22955286	2.8893626
0	0.774596	5.0215168	5.0380094	5.0737770
0.774596	-0.774596	0.4158858	0.5031764	0.4359446
0.774596	0	0.1585558	0.0014381	0.1377572
0.774596	0.774596	2.4214388	1.8343199	2.2514571

Table 2.2.1 The moments of enriched element shown in Figure 2.2.5 by computed with (a) symbolic, (b) before grid separation, and (c) after grid separation.

Table 2.2.1 shows the differences between the moments of integrand type 1 (i.e., $I_1^1, \dots, I_1^9$) of Figure 2.2.5 obtained by the symbolic, and numerical computation of four and nine nodal level set values respectively. The integration of (12) was performed in the reference domain r and s of the enriched element. The maximum relative error of each method is 13.12% and 99.1% respectively. We confirm that the error of the ground truth (i.e., symbolic computation of the moment fitting weight) with utilizing four nodal level set values significantly increases while nine nodal level set values are not. This clearly demonstrates the effect of grid separation.

2.3 Artificial neural network

In order to fully exploit the benefits of the selective enrichment and the moment fitting method as well as adaptive resolution of interface representation discussed in Chapter 2.2.2, efficient computation of weights for the given level set representation is required. However, the computation of such has a large memory footprint, and the ensuing computational load increases with respect to the number of enriched elements. This problem by no means is exacerbated when the number of enrichment functions increases (i.e., Heaviside function), or interface changes during analysis (i.e., topology optimization). The present section introduces an artificial neural network to emancipate the computational load of the moment fitting method by calculating the numerical parameters in the moments. The moment fitting method should be applied to the construction of the stiffness matrix, composed of several different types of the

integrand. This means it requires an independent calculation of the moment fitting weight repeatedly, which causes a heavy computational load. Therefore, we introduce an artificial neural network to reduce the calculation of the moment fitting weights, and also to compute each independent integrand type at once.

2.3.1 Data set preparation

Before the construction of the network, we first investigate the features of the input and output data of the network. we perform data processing for input data first. For the quadrilateral element, the shape function N_i is unchanged as mentioned in Chapter 2.2

$$N_1 = \frac{1}{4}(1-r)(1-s) \tag{17}$$

$$N_2 = \frac{1}{4}(1+r)(1-s) \tag{18}$$

$$N_3 = \frac{1}{4}(1+r)(1+s) \tag{19}$$

$$N_4 = \frac{1}{4}(1-r)(1+s) \tag{20}$$

where r and s is abscissas of the reference coordinates. The enrichment function F is, therefore, the function of the level sets of each node.

$$F(X) = f(\phi_1, \phi_2, \phi_3, \phi_4) \tag{21}$$

We use pre-defined quadrature points within the isoparametric element, the Lagrange polynomial through Gauss-Legendre point P^i is invariable. Therefore, the integrand of the moment fitting equation $H_j P^i$ is the function of the nodal level set values.

$$H_j P^i = g(\phi_1, \phi_2, \phi_3, \phi_4) \tag{22}$$

Figure 2.3.1 shows the process of input data. At this time, the nodal level set value should be in a certain

range for the simplification of data collection. Thus, we rescale each level set value into a range of ± 1 to avoid overrepresentation of certain interface layouts and to make the data well represent the distribution of the level set values. As illustrated in Figure 2.3.1, $\overrightarrow{\phi^*}$ represent the normalized level sets that maximum or minimum value of the original data becomes ± 1, respectively.

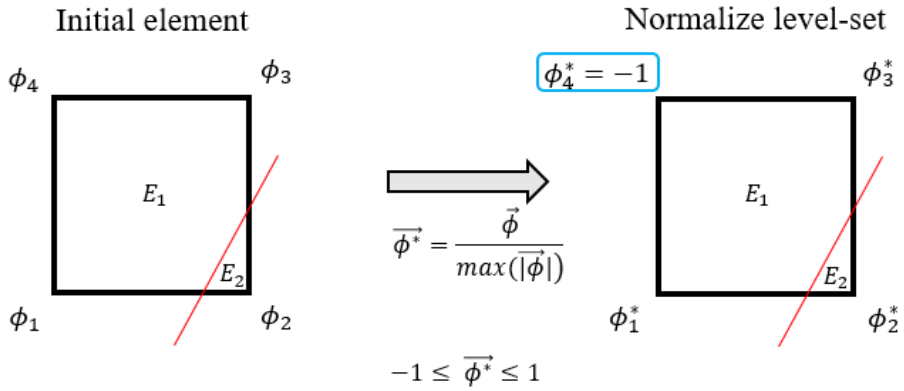

Figure 2.3.1 Normalization scheme of the nodal level set values.

The outputs of the network are the results of the pre-computed moment fitting method, and this process corresponds to offline time (i.e., excluded time from interpretation). As we pre-defined our quadrature point as 3×3 standard Gauss-Legendre points, a total of 99 integrations were needed for construction of the stiffness matrix $\boldsymbol{K}$ and force vector $\boldsymbol{f}$ in two-dimensional structures. For calculating outputs, we assume linear enrichment in enriched elements. The enriched element is then divided into sub elements, where case 1 contains pentagonal and triangular shaped sub elements and case 2 contains quadrilateral shaped sub elements as illustrates in Figure 2.3.2. For each sub-element, we can calculate each type of integrals with numerical computation, Gauss quadrature is used in this paper, the integrand is reduced to the XFEM procedure as well.

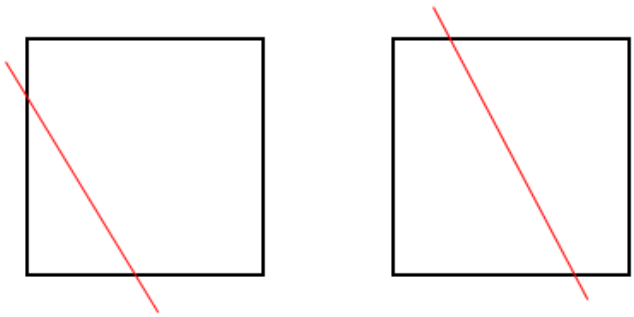

(a) Case 1 (b) Case 2

Figure 2.3.2 Feasible enrichment case. (a) case 1 involves pentagonal and triangular-shaped, and (b) case 2 involves two quadrilateral-shaped

In addition, we focus on the usage of a single network, regardless of the material properties. Assuming that the ratio of dissimilar material properties is already known, we consider the linear relation of the ratio of material properties and each type of integration I_j. For instance, the moments computation of the type 1 (i.e., I_1^i) is

$$\begin{aligned} I_1^i &= \int_{\Omega_e} H_1 P^i d\Omega_e = \int_{\Omega_e} E(X) P^i d\Omega_e \\ &= \int_{\Omega_1} E_1 P^i d\Omega_1 + \int_{\Omega_2} E_2 P^i d\Omega_2 \\ &= E_2 \left[\int_{\Omega_1} \frac{E_1}{E_2} P^i d\Omega_1 + \int_{\Omega_2} P^i d\Omega_2 \right] \\ &= E_2 \left[\frac{E_1}{E_2} \int_{\Omega_1} P^i d\Omega_1 + \int_{\Omega_2} P^i d\Omega_2 \right] \\ &= E_2 (r a_1^i + b_1^i) \end{aligned} \tag{23}$$

Where the ratio $r = E_1/E_2$. It is notable that other types contain the material distribution $E(X)$, the same procedure can be applied (i.e., $j = 3, \dots, 11$) while I_2, the material distribution can be assumed as zero. The enrichment function and its derivatives, $F(X)$ and $\nabla F(X)$, are remain in a_j^i and b_j^i in other type of integrands. Thus, it can be concluded that the entire moments require for interpretation has a linear relation with a_j^i and b_j^i. Thanks to the (23), the coefficients of the linear relationship of each integration according to the ratio of material properties were chosen as network outputs.

$$a_j^i = \int_{\Omega_1} T_j(X) P^i d\Omega_1 \tag{24}$$

$$b_j^i = \int_{\Omega_2} T_j(X) P^i d\Omega_2 \tag{25}$$

$$T_j(X) = \begin{cases} 1 & (j = 1) \\ F(X) & (j = 2) \\ \dfrac{H_j(X)}{E(X)} & (j = 3, \dots, 11) \end{cases} \tag{26}$$

After training, we can scale out of those output coefficients by the ratio of material properties reversely, realize the obtaining the moments within the element of arbitrary material distribution. We further investigate the trained network for concerning the Poisson`s ratio which we assumed to be constant. Previously, the integrand types are determined since the material distribution is expressed only by the Young`s modulus. We confirm that total 21 types of integrand are required after considering the Poisson`s ratio. The constitutive matrix $\boldsymbol{C}$ is constructed with $E(X)$ and $\nu(X)$ or $\mu(X)$ and $\lambda(X)$. Where μ and λ are lame constants, which defined under the plane strain condition as

$$\mu(X) = \frac{E(X)}{2(1+\nu(X))} \tag{27}$$

$$\lambda(X) = \frac{E(X)\nu(X)}{(1+\nu(X))(1-2\nu(X))} \tag{28}$$

After Galerkin procedure, the integrands of the stiffness matrix are then as follows

$$I_{j1} = \int_{\Omega_e} \mu(X) P^i d\Omega_e \tag{29}$$

$$I_{j2} = \int_{\Omega_e} \lambda(X) P^i d\Omega_e \tag{30}$$

$$\vdots$$

It is noteworthy that the weights of the integrand must be computed the same way, but such types in which Poisson's ratio is now considered can be represented using an identical trained network as (23).

$$I_{j1} = \int_{\Omega} \mu(X) P^i \, d\Omega \tag{31}$$

$$
\begin{aligned}
&= \int_{\Omega_1} \mu_1 P^i d\Omega_1 + \int_{\Omega_2} \mu_2 P^i d\Omega_2 \\
&= \mu_2 \left[\int_{\Omega_1} \frac{\mu_1}{\mu_2} P^i d\Omega_1 + \int_{\Omega_2} P^i d\Omega_2 \right] \\
&= \mu_2 \left[\rho \int_{\Omega_1} P^i d\Omega_1 + \int_{\Omega_2} P^i d\Omega_2 \right] \\
&= \mu_2 (\rho a_j^i + b_j^i)
\end{aligned}
$$

Where $\rho = \mu_1/\mu_2$ and μ_2, ρ is constant. Exactly the same procedure can be applied in I_{j2} either. Therefore, it is unburdened to use a trained network since the coefficients a_j^i and b_j^i have an identical form. In this investigation, we conclude that the types of the integrand in the moment fitting method depends on the variables in the constitutive equation. In this paper, we only consider the material distribution as the Young`s modulus $E(X)$ or Poisson`s ratio $\nu(X)$ in two-dimensional case, but it is straightforward to extend to three-dimensional problem. The key feature in utilizing the neural network for regressed the moments is it only depends on the shape of the enrichment (i.e., a_j^i and b_j^i). The integrand types can be chosen after formulate the constitutive equation.

Although there are two enrichment cases as illustrated in Figure 2.3.2, however, they are not distinguishable by the contents covered in this section. The integrands are greatly influenced by the assumed material distribution and thus changes significantly when the enrichment case changes, but not the linear parameter a_j^i and b_j^i. Therefore, we collect the data without distinguishing the enrichment cases.

The input data are 3 level set values of the enriched element that normalized at range ± 1, and training data are selected by segmenting the entire range of variables (i.e., $\phi_1^*, \phi_2^*, \phi_3^*$). However, sampled data with regular intervals was difficult to represent total cases. Accordingly, additional input data was extracted from the sections where outputs change rapidly. This rapid change occurs where the shape of enrichment alters from case 1 to case 2, because the integrand function $H_j P^i$ changes excessively. Thereby, we extract additional data to form a denser input field while further subdivision the section where the rapid change occurred. In addition, the rotational invariance of the network was implemented. Since the training samples are based on the quadrilateral element, depending on the alignment of the level sets for rotation (total 4 cases), the moment fitting weights have the same quantities, but in a different order. Because pre-defined Gauss quadrature point is symmetric and the shape function is unchanged. In that sense, we instill the rotational invariance in the network by training additional data

with a set of rotational data. The distribution of the sampled data is represented in Figure 2.3.3.

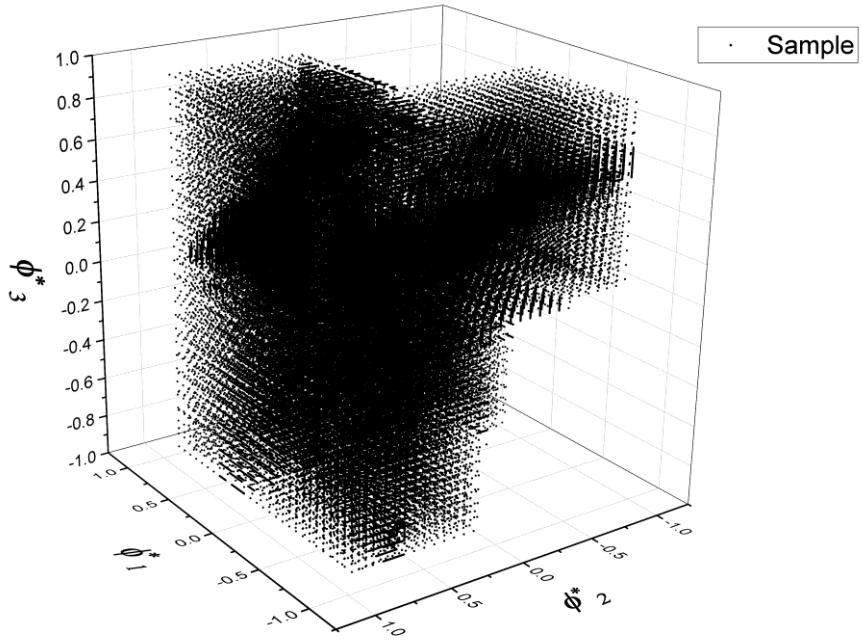

Figure 2.3.3 Distribution of the input data. Single point represent the normalized nodal level set, $\phi_1^*, \phi_2^*, \phi_3^*$. After dividing each variable into a certain section, further extraction of data is performed.

Furthermore, a few works including [13,17] addressed that the system is ill-conditioned when it contains intersected elements with the small ratio of the area or volume of each material occupied or a low area fraction occupied by different materials within the element. In the present work, poor regression results for the enriched element that has a low area fraction was found. Thus, we construct another feedforward network. In this process, the training data set are constructed only with elements that have an ill-posed condition system, setting the fraction of dissimilar area is below 5% based on the study of [13]. This allowed the application of ANN in the online calculation (i.e., analysis computing) for all enriched elements, regardless of its condition system.

2.3.2 Network architecture and performance

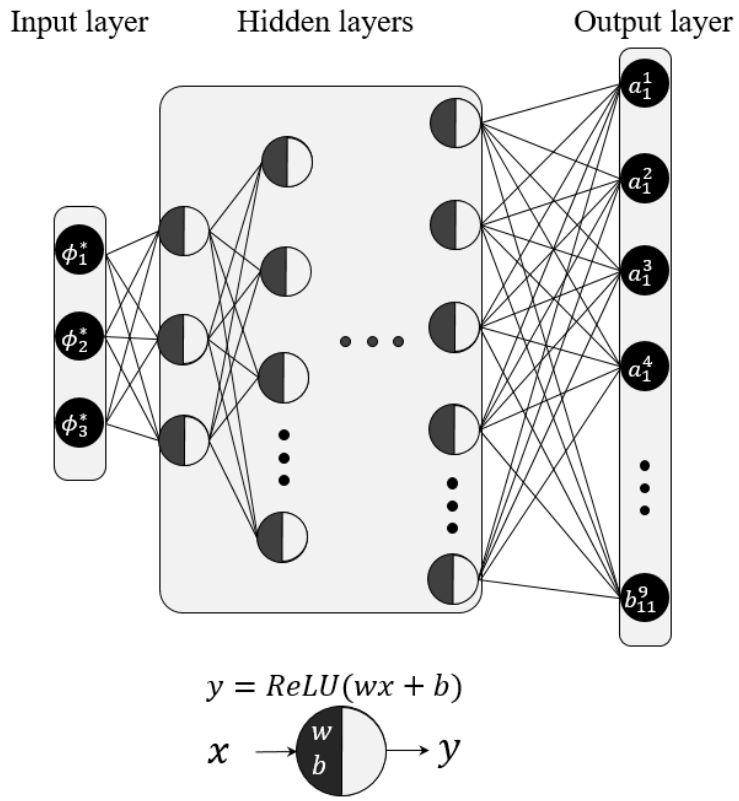

Figure 2.3.4 The architecture of the neural network, where regression of the relation of the level sets and the moments.

Figure 2.3.4 illustrates the neural network architecture for nonlinear regression herein. The feedforward method is used. As in Figure 2.3.4, the network input is normalized three level set values. While online computation, the required moments (i.e., $I_j^i = \int_\Omega H_j P^i d\Omega$) are computed by the outputs of the network, a_j^i and b_j^i. Here, the ReLU function was used as an activation function. The number of layers and nodes were adaptively determined to contain the output`s strong nonlinearity. We use the ADAM optimization method. The hyperparameters used in the present work is summarized in Table 2.3.1

Number of hidden layers	8
Number of nodes	3,26,140,380,420,540,600,800,198
Size of samples	176690
Batch size	Full batch
Activation function	ReLU
Learning rate	$10^{-3} \sim 10^{-5}$

Table 2.3.1 Hyperparameters of the regression networks. The same parameters were used for ill-conditioned element.

The loss of the network was measured by the mean square error of the numerically computed outputs. The graph of the loss is shown in Figure 2.3.5. The ratio of the training set and validation set is 7:3.

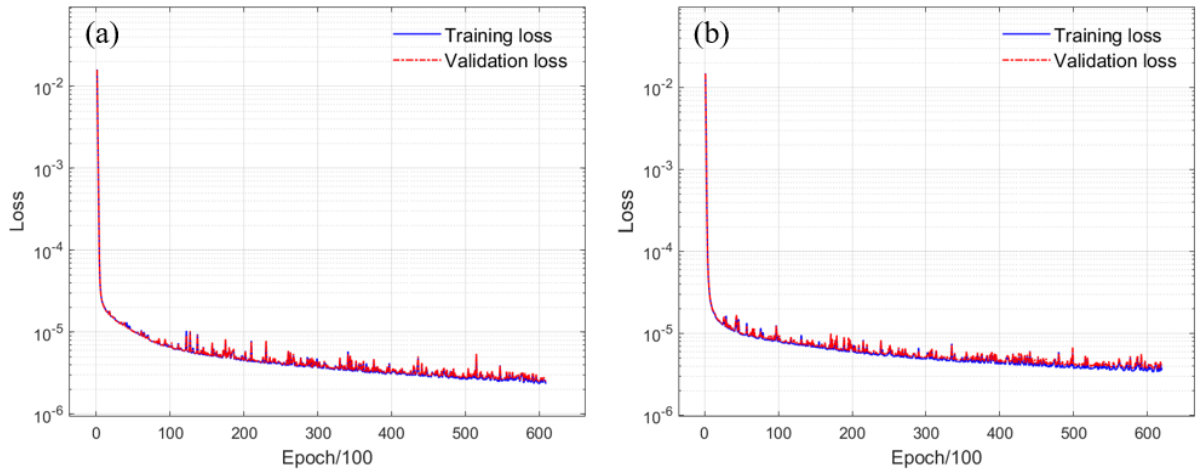

Figure 2.3.5 Training and validation loss of the network. (a) and (b) indicates the case of normalize level set to +1 and -1 respectively.

The loss of each network rapidly decreased as the epoch increases in the threshold of the training, before 5000 epochs, but we confirm that this amount of loss is not enough for applicable. After several experiments, we are able to train the network with sufficient loss, and the test of the results is required because the final goal for utilizing the network is not the outputs of the network but constructing a stiffness matrix using the output results. Therefore, we check our trained networks by calculating the moments of each type of integrand for arbitrary enriched elements. The moments of both symbolic and network-based calculation are shown in the Figure 2.3.6.

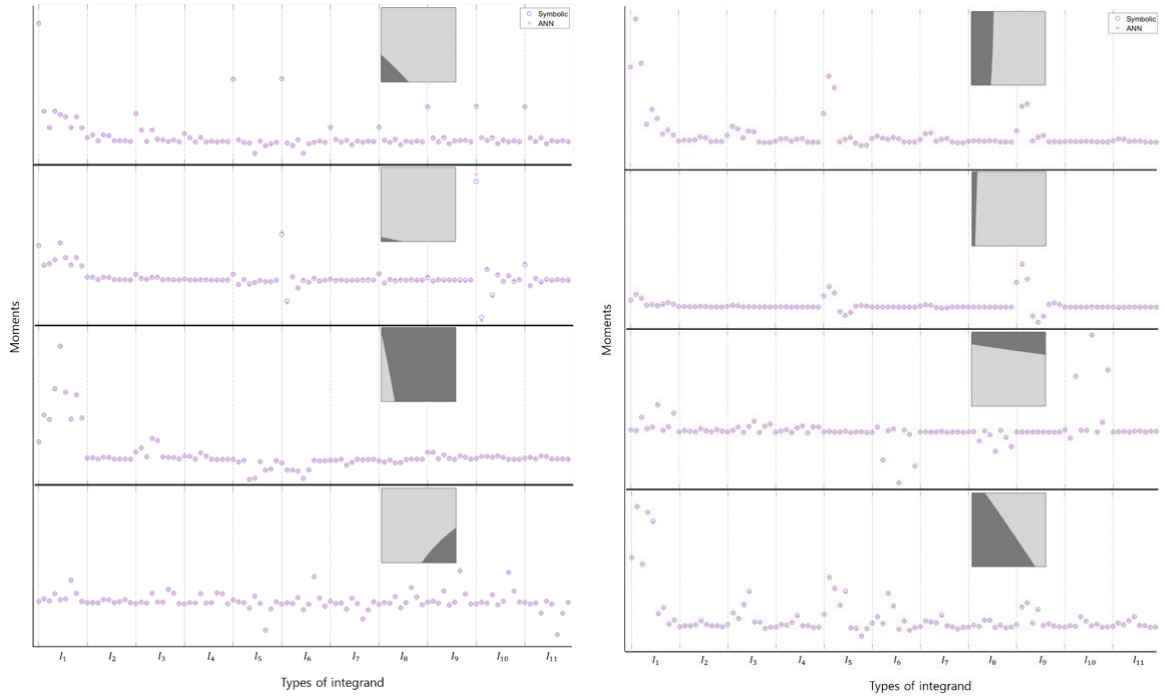

Figure 2.3.6 The moments by computed with symbolic (blue circle) and network-based (red cross) of several enriched elements for (a) case 1 and (b) case 2.

Herein, identical Poisson`s ratio but dissimilar material properties are assumed in the dark and light gray color in each of the elements. The moments computed by network-based (red cross) well resemble the symbolic calculated moments (blue circle). In online analysis, the predicted moment is used to obtain the weights according to each type of integral, which leads to the moment fitting quadrature. Thanks to the neural network, the moments can be calculated at once for various integrated without iterative loop calculation, and the integration of the complex functions is altered as neural networks from the numerical calculation. Therefore, the computational efficiency of online time can be guaranteed.

2.3.3 Proposed analysis method

The diagram of the general algorithm of the proposed method was illustrated.

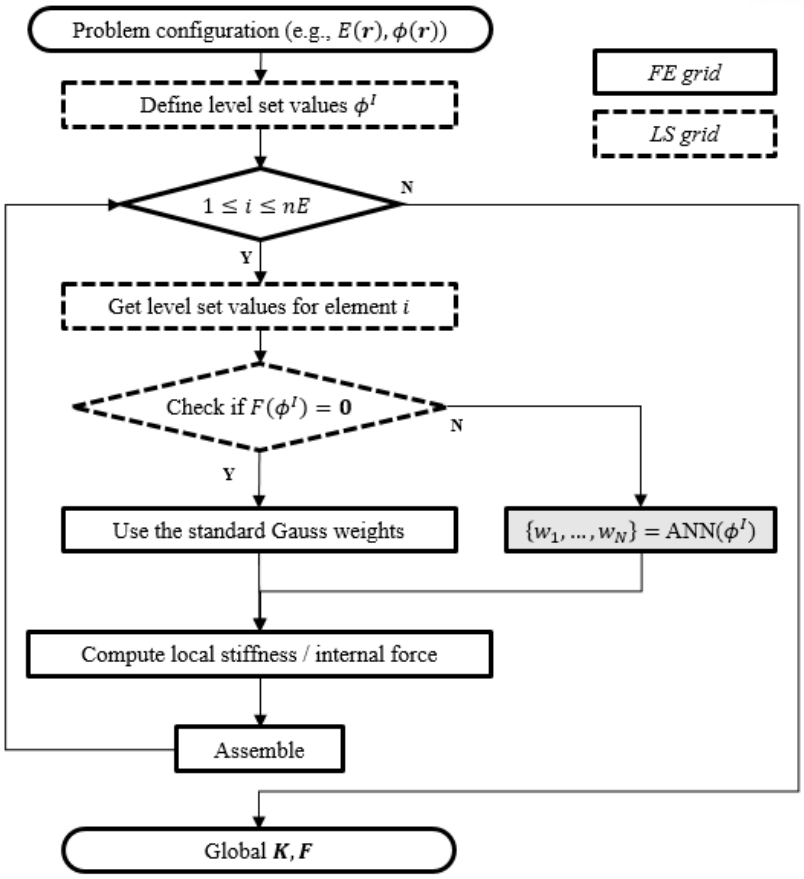

Figure 2.3.7 Algorithm of the finite element analysis utilizing the neural network. The level set grid and the finite element grid can be separated in dotted flow chart

After non-conforming meshing for the structure, the enrichment function F can be a distinguisher whether the element is enriched or not. If the element is enriched, obtaining the required moments can be done by the network regression on-the-fly process. If not, standard Gauss quadrature weights can be used. The increment of the first computational performance is taking place here, because the looped numerical computation for each integrand and Gauss quadrature point is no longer necessary but substitute with the simple regression process of matrix calculation. Nonetheless, the limitation is found herein, it initially requires a computation process that embeds the weights and the bias of the trained network into the program, which also may degrade the memory issues. However, in our numerical experience, the memory requires for implement the trained network takes about 10MB and no more than 0.5 seconds are needed, which is barely negligible. Second computational performance arises in the iterative problem (e.g., nonlinear, topology optimization) since the pre-computed moment fitting weights can be re-usable unless the level set values within the enriched element is constant. Further, as

shown in the diagram, we depart the level set grid and finite element grid in order to increase the accuracy without computational overhead. Utilizing the regression model for the adaptive resolution (LSM9 method) can be obtained a more accurate solution field with maintaining efficiency.

Chapter 3. Numerical examples

In this chapter, we present four numerical examples. The first two examples demonstrate the accuracy and efficiency of the proposed method by comparing the solutions obtained by the proposed method with respect to the ones by the well-known methods, including XFEM. Also, the last two serve to demonstrate the extensibility of the presented work: a hyperelasticity problem where the efficiency is conspicuous and a model with multiple types of inclusions where the neural network regression model is applied to more than two dissimilar structures. Each of the problems is curated in a way to show the efficacy of different features found in the work: the accuracy of the regression in the first, third, and last problem, the effect of grid separation in the second one.

`

3.1. Plate with a circular inclusion

As a benchmark problem, we demonstrate the accuracy of the proposed method, by solving a plane strain boundary value problem first presented in [10] illustrated in Figure 3.1.1.

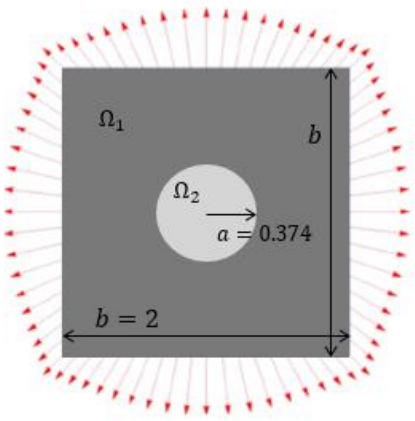

Figure 3.1.1 Boundary condition of circular inclusion

A square plate of length 2 is assumed to be composed of two dissimilar materials, each constitutes domain Ω_1 and Ω_2. The radius of circular inclusion a is 0.374. Young`s modulus and Poisson ratio of each material is 10, 1 and 0.3. Two domains are perfectly bonded. The Dirichlet boundary conditions and the corresponding exact solution with polar coordinate is given in (32)-(33) where λ_1, λ_2 and μ_1, μ_2 is the Lame constants in Ω_1 and Ω_2 respectively.

$$u_r(r) = \begin{cases} \left[\left(1 - \frac{b^2}{a^2}\right)\alpha + \frac{b^2}{a^2}\right] r, & 0 \le r \le a \\ \left(r - \frac{b^2}{r}\right)\alpha + \frac{b^2}{r}, & a \le r \le b \end{cases} \tag{32}$$

$$\alpha = \frac{(\lambda_1 + \mu_1 + \mu_2)b^2}{(\lambda_2 + \mu_2)a^2 + (\lambda_1 + \mu_1)(b^2 - a^2) + \mu_2 b^2} \tag{33}$$

To clearly present the effect of the proposed method, three other existing schemes solving weak discontinuity problems are also adopted; (1) Ersatz material, (2) XFEM, (3) MF (4) ANN+MF. In the ersatz material method, the modulus is evaluated at each Gauss-Legendre integration point and it is assumed to be linearly properties to the area of cut element. Figure 3.1.2 shows the L^2norm of the displacement error, obtained by different enrichment techniques.

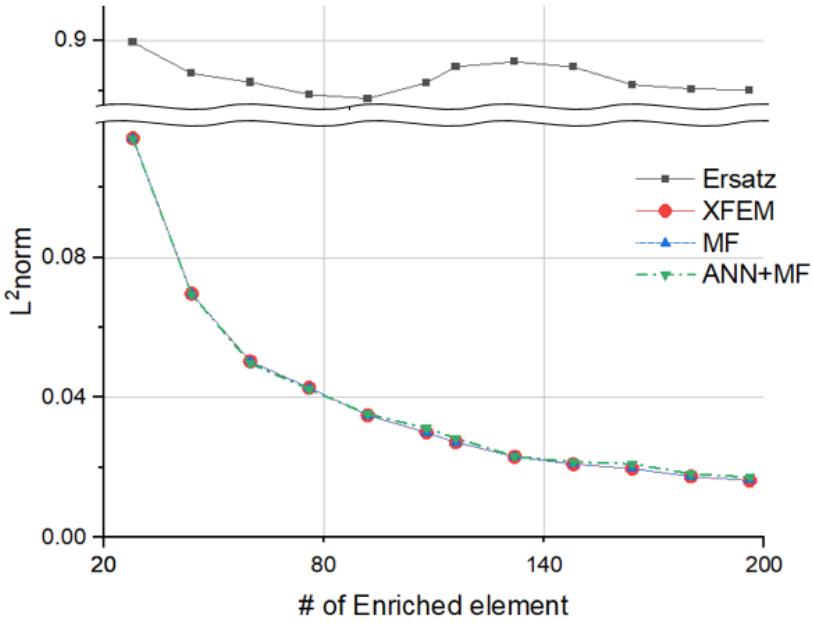

Figure 3.1.2 **L^2**norm of each method with the analytic solutions as the number of enriched elements increases.

The accuracy of the solution increases gradually as refining the interface (i.e., increasing the number of enriched elements). The error of the XFEM (red line) and the moment fitting method (green line) is exactly the same, although the calculation process of the stiffness matrix is different.

The Ersatz method, which takes up the least amount of integration time, has a considerable error around

the interface, as shown in Figure 3.1.3.

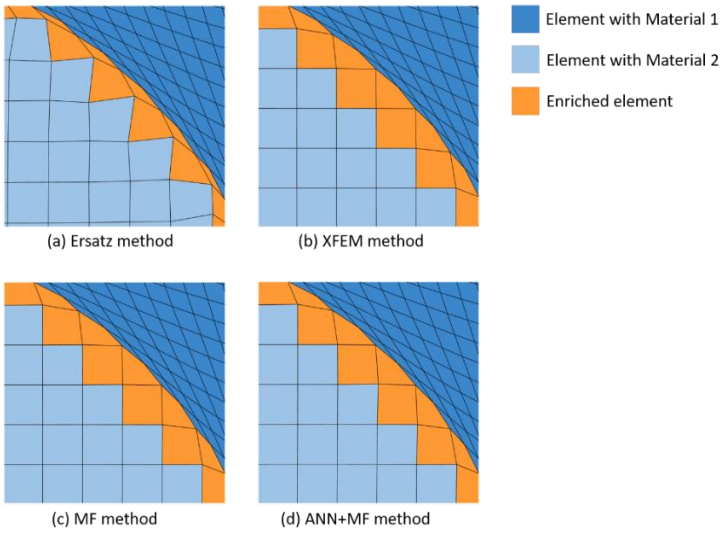

Figure 3.1.3 Mesh configuration around the interface for each method. (a) Ersatz, (b) XFEM, (c) MF, and (d) ANN+MF.

By replacing the ersatz method with other methods, which employ the enrichment strategy, such significant error around the material interface can be resolved. The MF and the ANN+MF method results agree very well: the maximum error 7.19%, which corresponds to the errors found at the moment fitting weights. The error does not increase further during stiffness matrix inversion.

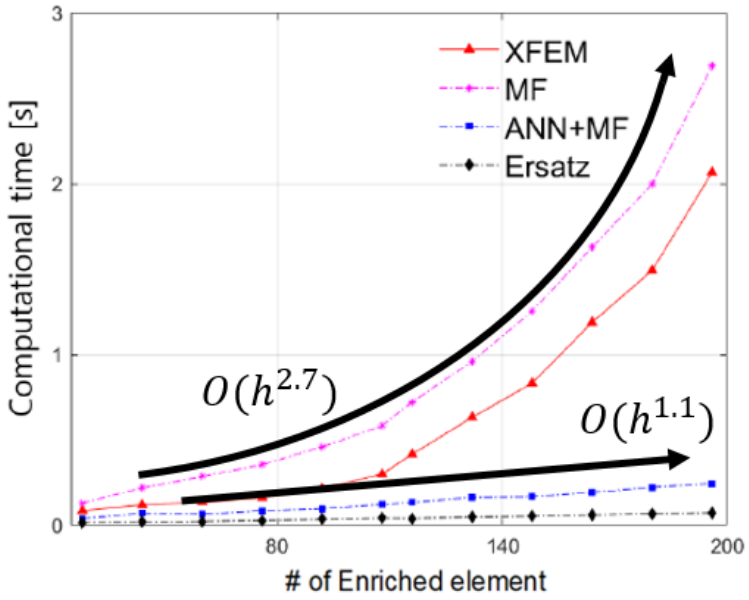

Figure 3.1.4 Amount of computational time of enriched elements for each method

Figure 3.1.4 represents the aggregated computational time spent during numerical integration of enriched elements that increases as the number of enriched elements increases. Ersatz method (black line) takes up minimum integration time and forms a baseline since it only requires standard Gauss-Legendre quadrature as a standard FEM. The MF method (magenta line) and the XFEM method (red line) require the sub-partitioning of the enriched elements and the numerical quadrature of the moments of (11). Therefore, as the number of partitioned domains and integration points increases, the integration time increases rapidly approximately $O(n^{2.7})$.

Notably, the computational time required for the ANN+MF method (blue line) is lower than that of MF and XFEM, because the ANN+MF method requires a simpler regression model of the corresponding moments by the level sets of enriched elements and trained networks and maintains the same number of integration points. Such agrees with the observation that the required integration time of ANN+MF increases almost linearly, indicating that additional computation load is spent only for the regression. This clearly demonstrates the efficiency of the proposed method. It is worth mentioning that this investigation is actually the first time where 2D, the moment fitting results are compared with the other works.

3.2 A cantilever beam with a dumbbell-shaped inclusion

The present problem addresses a dumbbell-shaped single inclusion problem, as illustrated in Figure 3.2.1. The geometry of the inclusion has a narrow neck at the center and gets as it approaches thicker each end. The curvatures, therefore, change drastically along the interface contour (green line), and such change inevitably increases the difficulty of interpretation, including the ambiguities discussed in Chapter 1.

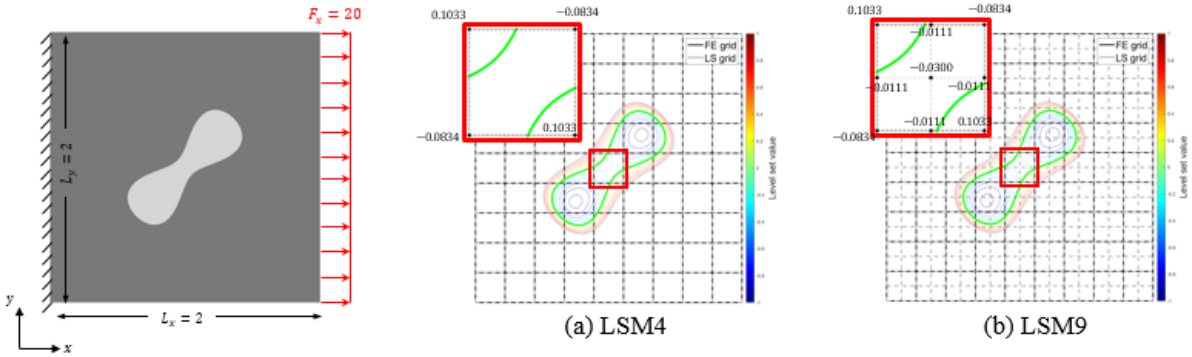

Figure 3.2.1 A cantilever beam with dumbbell-shaped inclusion problem and boundary condition. Same finite element grid (black solid line) is used but different level set grid (gray dashed line) is used; each FE grid finds (a) four level set nodes (LSM4), and (b) nine level set nodes (LSM9).

The material properties of inclusion has Young`s modulus $E_1 = 10$ at Ω_1 and $E_2 = 1$ with in Ω_2. The Poisson ratio of $\nu = 0.3$ is used for both materials. External force applied to the right end of Ω_2 with $F_x = 20$ to the x-direction. Fixed boundary condition is imposed to the left end. The contour of the level set function and grid are shown in Figure 3.2.1 (a) and (b). A green line, of isocontour of zero level set value represents the interface of the structure. The resolution of FE and the level set grids can be the same in Figure 3.2.1 (a), or be different as shown in (b). Throughout the example, the resolution of the level set grid is higher than that of the finite element grid, which is necessary since the accuracy is greatly deteriorated otherwise. Also, the ambiguity problem occurs in the center of the structure as marked red box in (a). However, the interpretation of such issue becomes clearly in (b), since we can utilize more level set values in enriched element. The efficacy of utilizing a higher number of level set nodes than the finite element nodes representing geometry in finer resolution is demonstrated in this example.

The internal Von-Mises stress of structures after employing the boundary conditions in Figure 3.2.1 is measured and compared to verify the solution field of each different method. The total number of DOF is 20000, and the only difference between each method is the approach of computing the stiffness matrix. In the LSM4 method, the moment fitting and selective enrichment approach is applied where the weighting factors are computed by the trained network. Contrary, in the LSM9 method, the weighting factors utilized with 9 nodal level set values are calculated in numerical computation.

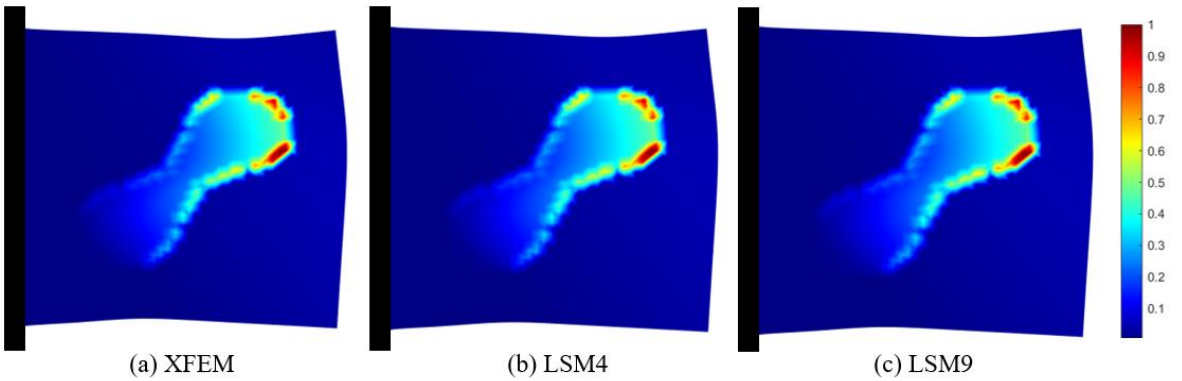

(a) XFEM (b) LSM4 (c) LSM9

Figure 3.2.2 Internal Von-Mises stress of structure in Figure 3.2.1 with computing each different methods (a) XFEM, (b) LSM4, and (c) LSM9

The maximum percent stress error difference of the LSM4 and LSM9 with XFEM is 1.97% and 1.75% respectively. Moreover, this example emphasizes the affective of the grid separation. To figure out the influence of grid separation, we select the different points where inner, outer, and the interface, observe the displacement of such points with respect to the number of DOFs. Figure 3.2.3 shows the displacement convergence of LSM4(black line) and LSM9(red line) with XFEM.

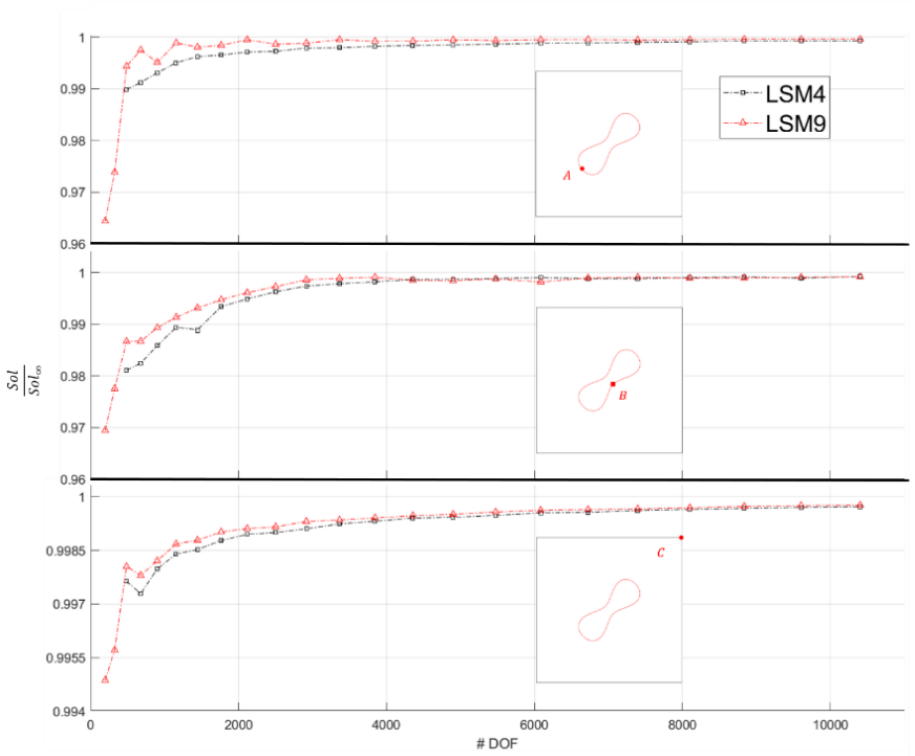

Figure 3.2.3 The convergence of LSM4 and LSM9 method while the number of DOFs increases. The Sol_∞ was obtained by high DOFs of XFEM.

Displacement of each different points A, B, and C are compared with the solution obtained by high DOFs of XFEM. During analysis, the moments regressed through the trained network are used in LSM4, whereas the numerically computed moments are used in LSM9. The solution of each method, LSM4 and LSM9 converge as the number of degree of freedom increases. If the total number of DOFs is lower than 484, which corresponds to a mesh of 11 by 11, the structure cannot be analyzed in a standard marching square method because of the ambiguity using the LSM4 scheme. On the other hand, the ambiguity is resolved in LSM9 in low resolution. In low DOFs, the interpretation of LSM9 shows better accuracy than that of LSM4, this is because the surface integration of FE grid becomes more accurate.

Additionally, the deviation between LSM4 and LSM9 is observed even when the number of DOF is about 500, where LSM9 converges to the accurate solution within 0.6956%. While LSM4 shows a larger error, 1.046% Therefore, it can be concluded that the overall accuracy increased even if the inaccuracy had not been for the ambiguity.

3.3 Nonlinear finite element analysis: hyperelasticity

This numerical example shows the vast efficient usage of the moment fitting method because the number of interpretation point remains and the weights are reused through the iteration solver. The problem setup is illustrated in Figure 3.3.1.

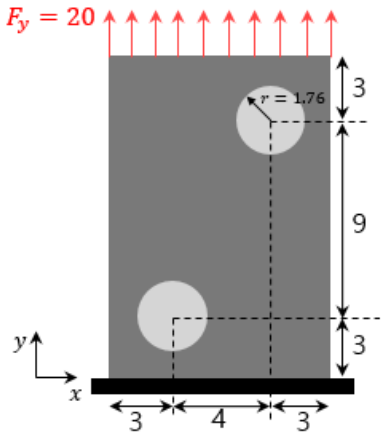

Figure 3.3.1 Two circular inclusions in a plate with dissimilar hyperelastic materials. Plate (dark gray) and inclusion (light gray) has material properties of $\boldsymbol{\mu_1}$ and $\boldsymbol{\lambda_1}$, $\boldsymbol{\mu_2}$ and $\boldsymbol{\lambda_2}$ respectively.

The dissimilar material properties are $\mu_1 = 2.083$ $\lambda_1 = 2.777$ $\mu_2 = 4.166$ $\lambda_2 = 1.388$, where μ and λ are Lame constants. The radius of inclusions are 1.76, and they are located as shown in Figure 3.3.1. Incompressible Neo-Hookean model is used for this example, where the energy potential is

$$W = \frac{G_0}{2}(I_1 - 3) + \frac{2}{K_0}(J-1)^2 \tag{34}$$

Where G_0 and K_0 are initial shear and bulk modulus respectively, I_1 is first deviatoric strain invariant, which is defined as $I_1 = s_1^2 + s_2^2 + s_3^2$, where s_i $(i = 1,2,3)$ is principle stretches. Since

we assumed incompressible Neo-Hookean material, $J = 1$. For analysis, the total Lagrangian formulation is adopted with Newton iteration solver, the number of steps is 5 is used for Newton iteration with the load control scheme. The convergence ratio is set to 10^{-8}.

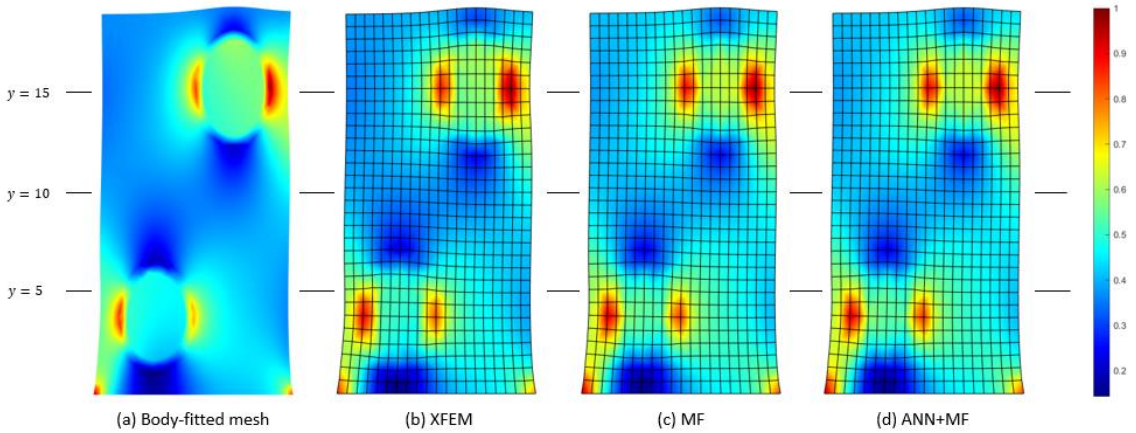

Figure 3.3.2 Strain energy distribution of deformed configuration. (a) Body-fitted mesh (b), (c), (d) non-conforming mesh with different methods

The analysis results of the given problem are shown in Figure 3.3.2 where strain energy is plotted to verify the accuracy of the solution. Nonlinearity is salient as the maximum displacement of the structure is 19.344, which roughly corresponds to 29 % of uniaxial deformation. The initial height of the structure $y = 15$, whereas the large deformation occurs as marked in Figure 3.3.2. For a, body-fitted mesh, Figure 3.3.2 (a), 7732 DOFs were found while a non-conforming mesh obtained in commercial program, ABAQUS 2020, finds 2604 DOFs. The maximum percentage error of strain energy between XFEM and ANN+MF method is 2.507%, and XFEM and MF method is 2.894%. It is worth noting that the pre-trained regression model is utilized without any change in the hyperelastic model as long as the same type of element is used. As mentioned in Chapter 2.3.1, the trained network returns different results according to the shape of the enrichment, regardless of the material properties. Thereby we demonstrate the extensibility of the proposed method in this numerical example.

The computation time of nonlinear problems with XFEM, MF, and ANN+MF methods are compared likewise in the first example. It is considered as the case where a dramatic increase of efficiency of the MF method would be shown. The computation time is calculated by the aggregating whole integration time of enriched elements while Newton iteration.

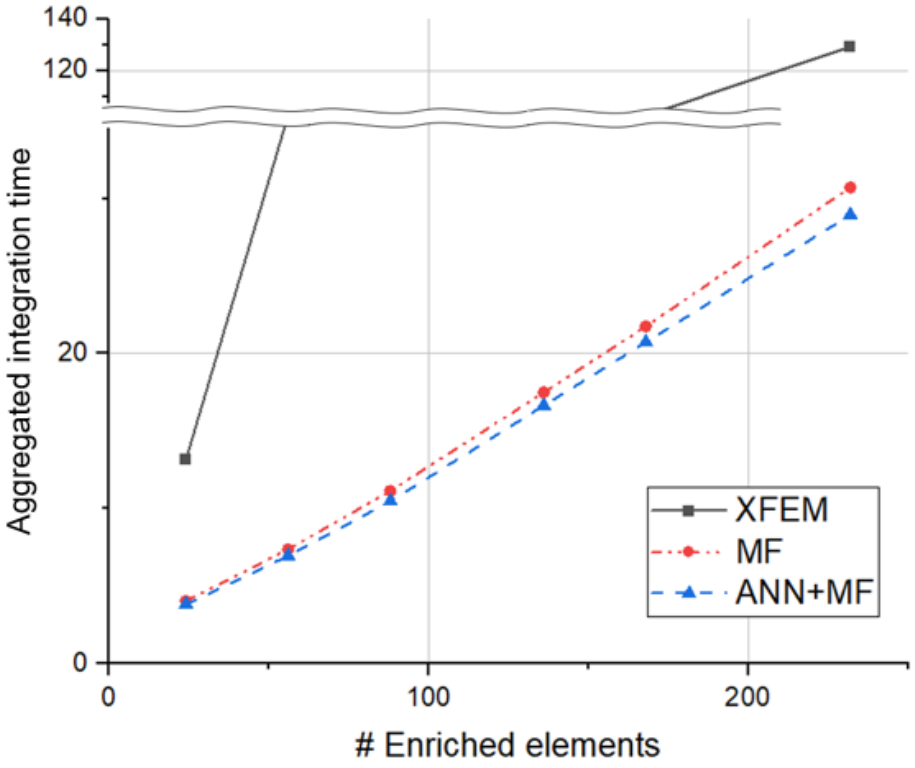

Figure 3.3.3 Comparison of aggregated integration time differences of enriched elements during iteration between XFEM, MF, and ANN+MF method.

As shown in Figure 3.3.3, there are dramatic differences in time spent during iteration between the MF-related methods and XFEM. This is because the system matrices and vector (i.e., global tangent stiffness and global residual vector) should be updated for each of the Newton-Raphson iteration steps. The rapid increase of computation time in the XFEM method is attributed to the increased number of sub-partitioning and quadrature function evaluations at each iteration. Meanwhile, in MF and ANN+MF methods, the computation time of the system matrices and vector is extremely shorter than XFEM, because the quadrature weights of each enriched element remain constant once obtained at the beginning of the iteration since the level sets of enriched elements remain during deformation. While using the MF-related method, the computational time decreases a maximum of 540.8%, a minimum of 357%, and an average of 450%. It is expected that considerable efficiency of the proposed method in the case of the nonlinear problem.

The difference between the MF and its ANN+MF method is comparably small as shown in Figure 3.3.3. The time difference is at maximum 1.76 seconds when the number of enriched elements is 232. This difference arises from the approach of getting moments: calculation time for numerical computation of

the moments compared to the regression model. Therefore, it can be concluded that the regression model would be more beneficial where the interface constantly changes during computation, (e.g., topology optimization) which is the forthcoming work of the authors.

3.4 A plate with multiple inclusions having different material properties.

To further demonstrate the extensibility of the proposed regression model, a plate with multiple inclusions is considered as the last numerical example. The configuration of the problem is illustrated in Figure 3.4.1

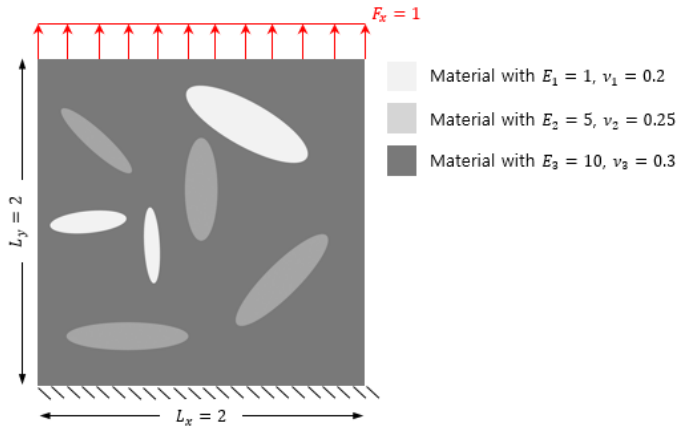

Figure 3.4.1 Plate with multiple inclusions and boundary condition.

In this numerical example, three different materials are employed. The interfaces thus are two types: one for where the interface containing Young`s modulus of $E_3 = 10$, $\nu_3 = 0.3$ in Ω_3 and $E_1 = 1$, $\nu_1 = 0.2$ in Ω_1 and the other where Ω_3 and $E_2 = 5$, $\nu_2 = 0.25$ in Ω_2. Nevertheless, a pre-trained regression model using a neural network can be applied regardless of the interface type. The external load F_y and fixed supported boundary condition is applied at the top and bottom of the structure respectively. To verify the solution, the Von-Mises stress of the structures solving with different methods are shown in Figure 3.4.2.

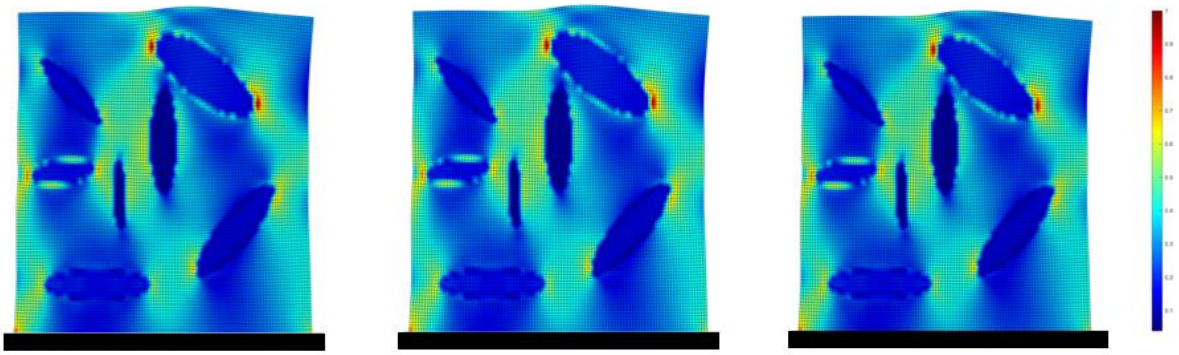

Figure 3.4.2 Von-Mises stress distribution of different methods; (a) XFEM (b) ANN+MF (c) LSM9

While analyze the enriched element with dissimilar materials, one pre-trained regression model was used for each interface as mentioned. The stress concentration of multi-inclusion structure utilizing different methods, maximum percent error of stress between XFEM and ANN+MF is 0.4% and XFEM and LSM9 is 0.52%. The computational costs of each example have only a slight difference (a few seconds) and are similar to the first example since it does not have an iterative calculation. Utilizing the LSM9 method, weights can be obtained similarly to desired weights because it has a higher resolution for the enriched element in case of the shape is curvy. In numerical experience, it was confirmed that the maximum percent error of stress is 0.31% where using LSM9 and XFEM that has doubled DOFs. This clearly indicates that we can obtain better interpretation results by maintaining the finite element grid without increasing the computing load when using the LSM9 method.

Furthermore, we measure the stress distribution around the interfaces, which is the major interest of multiphase structure. Figure 3.4.3 shows the Von-Mises stress within the cross sectional area $\overline{\boldsymbol{AB}}$, where $\overline{\boldsymbol{AB}}$ contains the major axes of the ellipse, that verified as stress concentration.

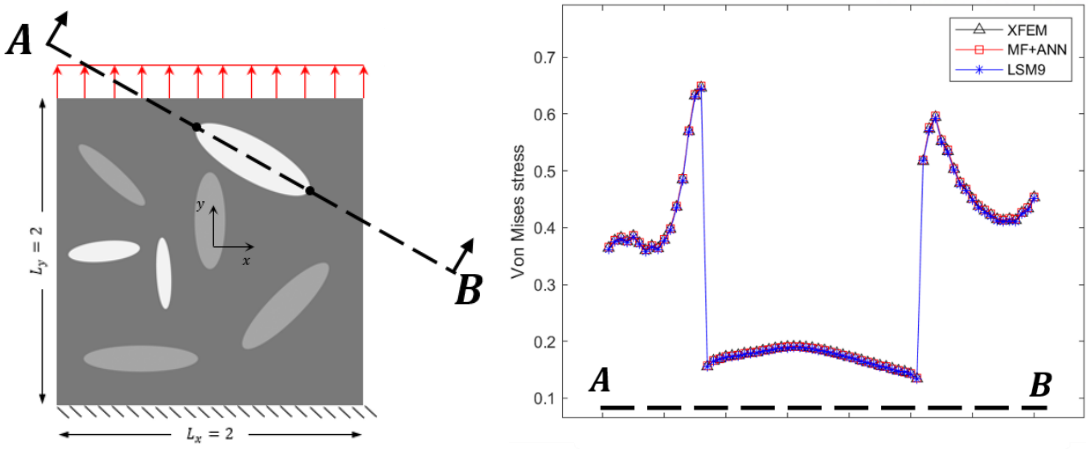

Figure 3.4.3 Von-Mises stress of cross sectional area $\overline{AB}$

The stress jump appears in the interface which is the feature of the weak discontinuity. The maximum percent error along the cross sectional area of the proposed method and LSM9 method with XFEM is 0.61% and 0.64% respectively. In the previous example, we investigate the extensibility of the proposed method by applying the hyperelastic material. Also in this example, it is suitable for the multiple cases of material interfaces regardless of their material properties. Therefore, the applicability is thereby demonstrated. We emphasize that this is because the trained network depends on the level sets of the enriched elements, also independent with material properties but linear parameters of the integrands.

In the first numerical example, we investigate the accuracy and efficiency of the proposed method, by comparing it with the traditional XFEM and Ersatz method. In the Ersatz method, a sufficient error around the interface was found, and also such error can be solved by applying the enrichment strategy. Further, the computational cost issue in the selective enrichment and the moment fitting method was solved by introducing an artificial neural network. In the second numerical example, the grid separation technique is addressed to increase the solution accuracy without increasing the computing overhead. We use the LSM9 method with numerically computed weights, nevertheless, it is straightforward that the neural network for the LSM9 method ensures the effect of the grid separation. In the third and fourth numerical examples, we demonstrate the extensibility and applicability of the proposed method with various material properties such as hyperelastic material and multiple dissimilar interfaces.

Chapter 4. Conclusion

In the present work, we propose a moment fitting method enhanced by a neural network that enables accurate and efficient analysis of the multiphase structures using non-conforming mesh. The enrichment technique, which the choice of enrichment function has a form of a ridged centered, first proposed by Moës [9] is used herein. The integration of such enriched elements requires heavy computational costs due to the increment of quadrature points, thus we use the moment fitting method combined with the selective enrichment technique. Through this approach, integrating and constructing the stiffness matrix of the discontinuous material using the moment fitting method is enhanced by a neural network. The calculation of the moments is done in the offline stage and regressed on-the-fly in the finite element analysis. The computational overhead is thereby marginal while securing the accuracy of the desired solution. We confirm the computational efficiency increases in the entire finite element analysis by utilizing the neural network model. We also increase the accuracy of desired solution space by detaching the finite element grid and level set grid in order to make better details of the enrichment, since the resolution of finite element grid is insufficient to represent the exact enrichment. As a result, the weighting factors of the moment fitting method can be more accurate while grid separation, since the precise representation of the enriched element is possible. Several numerical examples, both linear and nonlinear, are demonstrated to verify the proposed method's accuracy and efficiency. Moreover, a few examples, such as having a narrow neck or multiple inclusion problems, are demonstrated to substantiate the extensibility and applicability of the proposed method.

As a future work, the proposed method can be applied for the increment of the computing efficiency in nonlinear topology optimization or rapid computation in the iterative calculation in the homogenization method. Expanding the current research up to three-dimensional and employing such applications can be also considered. In addition, realizing the network of LSM9 method, numerically calculated in the present work, could be increasing the solution accuracy without any computing overhead, expecting the global utilization of the proposed method.

References

[1] Melenk, J. M., & Babuška, I. The partition of unity finite element method: Basic theory and applications. *Computer Methods in Applied Mechanics and Engineering*. **1996**. 139(1–4), 289–314.

[2] Babuška, I., & Melenk, J. M. The partition of unity method. *International Journal for Numerical Methods in Engineering*. **1997**. 40(4), 727–758.

[3] Belytschko, T., & Black, T. Elastic crack growth in finite elements with minimal remeshing. *International Journal for Numerical Methods in Engineering*. **1999**. 45(5), 601–620.

[4] Strouboulis, T., Copps, K., & Babuška, I. Computational mechanics advances. The generalized finite element method. *Computer Methods in Applied Mechanics and Engineering*. **2001**. 190(32–33), 4081–4193.

[5] Strouboulis, T., Babuška, I., & Copps, K. The design and analysis of the Generalized Finite Element Method. *Computer Methods in Applied Mechanics and Engineering*. **2002**. 181(1–3), 43–69.

[6] Belytschko, T., Moës, N., Usui, S., & Parimi, C. Arbitrary discontinuities in finite elements. *International Journal for Numerical Methods in Engineering*. **2001**. 50(4), 993–1013.

[7] Stolarska, M., Chopp, D. L., Mos, N., & Belytschko, T. Modelling crack growth by level sets in the extended finite element method. *International Journal for Numerical Methods in Engineering.* **2001**. 51(8), 943–960.

[8] Moës, N., Dolbow, J., & Belytschko, T. A finite element method for crack growth without remeshing. *International Journal for Numerical Methods in Engineering*. **1999**. 46(1), 131–150.

[9] Moës, N., Cloirec, M., Cartraud, P., & Remacle, J. F. A computational approach to handle complex microstructure geometries. *Computer Methods in Applied Mechanics and Engineering*. **2003**. 192(28–30), 3163–3177.

[10] Sukumar, N., Chopp, D. L., Moës, N., & Belytschko, T. Modeling holes and inclusions by level sets in the extended finite-element method. *Computer Methods in Applied Mechanics and Engineering*. **2001**. 190(46–47), 6183–6200.

[11] Sukumar, N., Moës, N., Moran, B., & Belytschko, T. Extended finite element method for three-dimensional crack modelling. *International Journal for Numerical Methods in Engineering*. **2000**. 48(11), 1549–1570.

[12] Aragón, A. M., & Simone, A. The Discontinuity-Enriched Finite Element Method. *International Journal for Numerical Methods in Engineering.* **2017**. 112(11), 1589–1613.

[13] Lang, C., Makhija, D., Doostan, A., & Maute, K. A simple and efficient preconditioning scheme for heaviside enriched XFEM. *Computational Mechanics*. **2014**. 54(5), 1357–1374.

[14] Béchet, E., Minnebo, H., Moës, N., & Burgardt, B. Improved implementation and robustness study of the X-FEM for stress analysis around cracks. *International Journal for Numerical Methods in Engineering*. **2005**. 64(8), 1033–1056.

[15] Sauerland, H., & Fries, T. P. The stable XFEM for two-phase flows. *Computers and Fluids*. **2013**. 87, 41–49.

[16] Babuška, I., & Banerjee, U. Stable Generalized Finite Element Method (SGFEM). *Computer Methods in Applied Mechanics and Engineering*. **2012**. 201–204, 91–111.

[17] Fries T.P. The intrinsic XFEM for two-fluid flows. *International Journal for numerical methods in Fluids*. **2009**. 60, 437-471

[18] Fries T.P. A corrected XFEM approximation without problems in blending elements. *International Journal for numerical Methods in Engineering*. **2008**. 75, 503-532

[19] S. E. Mousavi, H. X. and N. S. Generalized Gaussian quadrature rules on arbitrary polygons. International, February. **2012**. 1102–1119.

[20] J. N. Lyness, D. Jespersen. Moderate Degree Symmetric Quadrature Rules for the Triangle. *IMA Journal of Applied Mathematics.* **1975**. 15(1), 19–32,

[21] Dunavant DA. High degree efficient symmetrical Gaussian quadrature rules for the triangle. *Int J Numerial Methods*. **1985**. Eng 21:1129–1148

[22] Mousavi, S. E., & Sukumar, N. Numerical integration of polynomials and discontinuous functions on irregular convex polygons and polyhedrons. *Computational Mechanics*. **2011**. 47(5), 535–554.

[23] B. Müller, F. Kummer, and M. Oberlack. Highly accurate surface and volume integration on implicit domains by means of moment-fitting. *International Journal for Numerical Methods in Engineering.* **2013**. 1102–1119.

[24] Hubrich, S. Numerical integration in the finite cell method based on moment-fitting. **2015**. July.

[25] Joulaian, M., Hubrich, S., & Düster, A. Numerical integration of discontinuities on arbitrary domains based on moment fitting. *Computational Mechanics*. **2016**. 57(6), 979–999.

[26] Hubrich, S., Di Stolfo, P., Kudela, L., Kollmannsberger, S., Rank, E., Schröder, A., & Düster, A. Numerical integration of discontinuous functions: moment fitting and smart octree. *Computational Mechanics*. **2017**. 60(5), 863–881.

[27] Hubrich, S., & Düster, A. Numerical integration for nonlinear problems of the finite cell method using an adaptive scheme based on moment fitting. *Computers and Mathematics with Applications.* **2019**. 77(7), 1983–1997.

[28] Thiagarajan, V., & Shapiro, V. Adaptively Weighted Numerical Integration in the Finite Cell Method. *Computer Methods in Applied Mechanics and Engineering.* **2016**. 311, 250–279.

[29] Zhang, Z., Jiang, W., Dolbow, J. E., & Spencer, B. W. A modified moment-fitted integration scheme for X-FEM applications with history-dependent material data. *Computational Mechanics*. **2018**. 62(2), 233–252.

[30] Bui, H. G., Schillinger, D., & Meschke, G. Efficient cut-cell quadrature based on moment fitting for materially nonlinear analysis. *Computer Methods in Applied Mechanics and Engineering*. **2020**. 366.

[31] Düster, A., & Allix, O. Selective enrichment of moment fitting and application to cut finite elements and cells. *Computational Mechanics*. **2020**. 65(2), 429–450.

[32] Im, S., Kim, H., Kim, W., & Cho, M. Neural network constitutive model for crystal structures. *Computational Mechanics*. **2021**. 67(1), 185–206.

[33] Li, W., Bazant, M. Z., & Zhu, J. A physics-guided neural network framework for elastic plates: Comparison of governing equations-based and energy-based approaches. *Computer Methods in Applied Mechanics and Engineering*. **2021**. 383.

[34] Xiao, G., Wen, L., & Tian, R. Arbitrary 3D crack propagation with Improved XFEM: Accurate and efficient crack geometries. *Computer Methods in Applied Mechanics and Engineering*. **2021**. 377, 113659.

[35] Kim, J. H., & Kim, Y. H. A predictor-corrector method for structural nonlinear analysis. *Computer Methods in Applied Mechanics and Engineering.* **2001**. 191(8–10), 959–974.